2007

Synthesis, Characterization, and Spectroscopy of Model Molybdopterin Complexes

Sharon J. Nieter Burgmayer
sburgmay@brynmawr.edu

Mary Kim

Rebecca Petit

Amy Rothkopf

Shadia BelHamdounia

See next page for additional authors

Custom Citation

Sharon J. Nieter Burgmayer, Mary Kim, Rebecca Petit, Amy Rothkopf, Alison Kim, Shadia BelHamdounia, Ying Hou, Arpad Somogyi, Diana Habel-Rodriguezc, Antonio Williams, Martin L. Kirk, "Synthesis, characterization, and spectroscopy of model molybdopterin complexes," *Journal of Inorganic Biochemistry* 2007 Nov;101(11-12):1601-16.

Authors
Sharon J. Nieter Burgmayer, Mary Kim, Rebecca Petit, Amy Rothkopf, Shadia BelHamdounia, Ying Hou, Arpad Somogyi, Diana Habel-Rodriguez, Antonio Williams, and Martin L. Kirk

Synthesis, Characterization, and Spectroscopy of Model Molybdopterin Complexes ‡

Sharon J. Nieter Burgmayer[*1], Mary Kim[1], Rebecca Petit[1], Amy Rothkopf[1], Alison Kim[1], Shadia BelHamdounia[1], Ying Hou[1], Arpad Somogyi[2], Diana Habel-Rodriguez[3], Antonio Williams[3], and Martin L. Kirk[*3]

[1]Department of Chemistry, Bryn Mawr College, Bryn Mawr, PA 19010

[2]Department of Chemistry, University of Arizona, Tucson, Arizona 85721-0041

[3]Department of Chemistry and Chemical Biology, The University of New Mexico, MSC03 2060, 1 University of New Mexico, Albuquerque, New Mexico 87131-0001

keywords:

molybdenum cofactor, pyranopterin, magnetic circular dichroism, electron paramagnetic resonance, dithiolene, bonding,

---

* *corresponding author:*

Email: sburgmay@brynmawr.edu, mkirk@unm.edu

FAX: 1-610-526-5086(SJNB), 1-(505) 277-2609 (MLK)

‡ Dedicated to the memory of Edward I. Stiefel

Abstract

The preparation and characterization of new model complexes for the molybdenum cofactor are reported. The new models are distinctive for the inclusion of pterin-substituted dithiolene chelates and have the formulation Tp*MoX(pterin-R-dithiolene) (Tp* = tris(3,5,-dimethylpyrazolyl)borate), X= O, S, R= aryl or –C(OH)(CH_3)$_2$). Syntheses of Mo(4+) and (5+) complexes of two pterin-dithiolene derivatives as both oxo and sulfido compounds, and improved syntheses for pterinyl alkynes and [Et_4N][Tp*Mo^{IV}(S)S_4] reagents are described. Characterization methods include electrospray ionization mass spectrometry, electrochemistry, infrared spectroscopy, electron paramagnetic resonance and magnetic circular dichroism. Cyclic voltammetry reveals that the Mo(5+/4+) reduction potential is intermediate between that for dithiolene with electron-withdrawing substituents and simple dithiolate chelates. Electron paramagnetic resonance and magnetic circular dichroism of Mo(5+) complexes where X = O, R = aryl indicates that the molybdenum environment in the new models is electronically similar to that in Tp*MoO(benzenedithiolate).

Introduction

For decades the identity of the molybdenum cofactor—the catalytic site in pyranopterin molybdenum enzymes—was sought through studies of the molybdenum enzymes and through synthetic efforts to manufacture compounds that reproduce key spectroscopic, structural, and reactivity properties of the catalytic Mo center. The significance of the molybdenum cofactor (Moco) has grown as awareness that at least one, and often several, Mo enzymes are required within every living organism. From a global perspective, molybdenum enzymes play essential roles in cycling the elements carbon, nitrogen and sulfur in processes largely carried out by bacteria [1-4]. Plants in the ecosystem depend on several molybdenum enzymes for their growth [5-8]. From a human perspective, three molybdoenzymes—sulfite oxidase, xanthine oxidase and aldehyde oxidase— are essential for proper health. In the extreme cases where genetic errors prevent the biosynthesis of functional molybdoenzymes, the resultant neurological problems are typically fatal [9-12].

In 1996 X-ray crystal structures of oxidized and reduced forms of dimethyl sulfoxide reductase (DMSOR) provided key structural details revealing the nature of Moco [13]. Consistent with proposals based on earlier spectroscopic studies, Moco from oxidized DMSOR comprised a single Mo atom coordinated by two dithiolene chelates and a single terminal oxo ligand. The dithiolene chelate found in DMSOR is now recognized as the unique ligand required by all Mo and W enzymes [14,15]. It is currently referred to as either molybdopterin or pyranopterin-ene-dithiolate. As both names indicate, this special chelate for Mo and W consists of a pterin structure fused to a pyran ring bearing an exocyclic dithiolene group that is the site of metal coordination (Fig.1).

Figure 1

The dithiolene chelate primarily determines the electronic characteristics responsible for the spectroscopic and certain reactivity properties of the Mo and W cofactors, a conclusion based on multiple studies of enzymes and model compounds. The dithiolene serves as an electronic buffer to modulate electron density changes at Mo during electron transfer reactions [16]. The orientation of the oxo ligand *cis* to the dithiolene chelate appears capable of functioning as an "oxo-gate" to isolate a specific orbital (d_{xy}) for electron transfer reactions [17]. The presence of two dithiolenes is key to the somewhat unusual mono-oxo-Mo(6+) and des-oxo-Mo(4+) units found in enzymes of the DMSOR family[18-19].

The importance of the dithiolene moiety notwithstanding, we have been intrigued with the role and potential reactivity of the pterin portion of Moco. We [20-24] and others [25-26] have studied the redox interplay between pterins and transition metals, including Mo. Reduced pterins react with many oxidized Mo(6+) complexes to produce Mo-coordinated pterin compounds where the electronic distribution is highly covalent [24]. In this regard, reduced pterin, like the 1,2-ene-dithiolate structure, is prone to form valence isomers. Evidence for pterin involvement in processes affecting the electronic distribution within Mo-chelated molybdopterin has recently been demonstrated in the recent X-ray structure of E. coli nitrate reductase [27]. This structure shows that one of the two molybdopterin ligands at the catalytic Mo site is in an unprecedented pyran ring-opened form that is highly suggestive of pterin involved in different redox forms in this enzyme.

Our curiosity about the pterin piece of Moco has driven a program to synthesize Mo compounds having dithiolene ligands substituted by a pterin. With such a ligand, redox reactions on the model system could be explored. Within our larger program to synthesize and characterize Mo complexes containing the pterinyl-dithiolene ligand, we have explored preparations of both *mono*- and *bis*-pterin-dithiolene complexes where the molybdenum is in both Mo(4+) and Mo(5+) oxidation states. In the work reported here, the coupling reactions of a molybdenum tetrasulfide reagent, $[Tp^*Mo^{IV}(O/S)(S_4)]^-$ (Tp* is *tris*(3,5-dimethylpyrazolyl)borate) with alkynes that directly produce chelated pterin-dithiolene ligands is described. The new models complexes obtained have the general formula, $[Tp^*Mo(O/S)(\text{pterin-dithiolene})]^{1-,0}$, in both Mo(4+) and (5+) oxidation states. Described in this work is the characterization of the purified Mo(5+) species by electrospray ionization mass spectrometry, electrochemistry, infrared spectroscopy, electron paramagnetic resonance and magnetic circular dichroism.

Experimental

Materials. All reagents and HPLC-grade solvents were purchased from Aldrich Chemical Company. $[Et_4N][Tp^*Mo^0(CO)_3]$ (Tp* is *tris*(3,5-dimethylpyrazolyl)borate) was prepared according to Curtis [28]. Reactions were conducted under anaerobic conditions using standard Schlenk techniques and all solvents were dried and deaerated immediately prior to use by stirring over activated alumina under N_2.
Methods. ^1H NMR spectra were taken on a Bruker 300 MHz FT-NMR Spectrometer. Chemical shifts were reported in parts per million (ppm) from a standard internal tetramethylsilane (TMS)reference. The

splitting of proton resonances in the reported ^{1}H NMR spectra are defined as s = singlet, d = doublet, t = triplet, m = multiplet. Fourier transform infrared (FTIR) spectra were obtained on Perkin-Elmer Model 2000 FT-IR Spectrometer from samples that were prepared as KBr pellets. Electrochemical analysis by cyclic voltammetry was done using a BioAnalytical Systems CV50 system, using TEAP as the electrolyte in acetonitrile, a platinum working and auxiliary electrodes and Ag/AgCl as reference electrode. All potentials are referenced to internal ferrocene whose potential is +0.40 vs. a Ag/AgCl reference electrode.

2-Pivaloyl-6-chloropterin. 6-chloropterin (1.82 g, 9.2 mmol) and 4-dimethylamino-pyridine (DMAP) (0.076g, 0.62 mmol) were loaded in a 2-neck Schlenk flask and purged under N_2(g) for at least four evacuation/refill cycles. Trimethyl acetic anhydride (3.9 mL) and anhydrous dimethylformamide (DMF) (39.2 mL) were dried by stirring over activated alumina then added by cannula to the deaerated reagents. The solution was heated at ~115^{o}C for 4 h during which time the solution color gradually changed from pale yellow to dark brown. After cooling to ambient temperature, the DMF solvent was removed by vacuum distillation to leave a dark orange solid. Product purification with chromatography (silica gel) used 2% methanol in dichloromethane as eluant. UV irradiation was used to track the ultramarine blue fluorescence of the product. Rotary evaporation of these fluorescent fractions produced a cream-colored solid in 96% yield. ^{1}H NMR ($CDCl_3$) δ (ppm) 12.67 (1H, s, NH), 8.82 (1H, s, CH), 8.04 (1H, s, NH), 1.33 (9H, s, t-Bu). Anal. Calcd for C11H12N5O2Cl: C, 46.90; H, 4.29. Found: C, 46.48; H, 4.26.

2-Pivaloyl-6-(3-hydroxybutyne)pterin (BOPP). 2-pivaloyl-6-chloropterin (1.00 g, 3.55 mmol), copper (I) iodide (0.095 g , 0.499 mmol), palladium (II) acetate (0.102 g, 0.454 mmol), and 1,1'-*bis*(diphenylphosphino)-ferrocene (0.254 g, 0.458 mmol) were loaded in a Schlenk flask and purged by several cycles of evacuation/ N_2(g) refill. Acetonitrile (25 mL), dried over activated Al_2O_3 and bubbled with N_2(g), was added via cannula. The solution stirred for 10 min, then 3-butyn-2-ol (5 mL) and triethyl amine (10 mL) were added via syringe and the mixture stirred again for 10 min. The reaction was warmed at 45 deg C for 3 hours, then cooled to room temperature and the acetonitrile solvent evaporated. The crude product was dissolved in dichloromethane and purified by column chromatography on silica gel eluting with 2% methanol in dichloromethane. Product elution was monitored using UV irradiation to track the blue fluorescent product. Rotary evaporation of fluorescent fractions containing product gave a pale tan solid in 90% yield. ^{1}H NMR ($CDCl_3$) δ (ppm): 12.45 (1H, s, NH), 8.87 (1H, s, CH), 8.48 (1H, s, NH), 4.63 (1H, m, CH), 2.12 (3H, d, CH_3),1.36 (9H, s, t-Bu). Anal. Calcd for C15H17N5O3: C, 57.13; H,

4.43. Found: C, 56.62; H, 4.44. MS (HRESI) *m/z* 316.1413 (calcd for [M+H] 316.1410) . FT-IR (cm^{-1}): ν(O-H) 3466, ν(N-H) 3186, 3201, 3119, ν(C≡C) 2224, ν(C=O) 1687, 1616, ν(C=N) 1555, 1440.

2-Pivaloyl-6-acetylethynyl pterin (AEP). Jones reagent was prepared by dissolving chromium (VI) oxide (3.5g, 35 mmol) in a solution of 12 M sulfuric acid (3.25 mL) and distilled water (9.25 mL) and chilled in the refrigerator prior to use. BOPP (0.3 g, 0.952 mmol) was dissolved in acetone (11.5 mL) chilled in an ice bath. 1 mL of chilled Jones reagent was added dropwise to the AEPa solution. Any aggregates that formed were removed, crushed in chilled acetone to release trapped product and then returned to the solution. The reaction was stirred for 20 minutes while chilled in an ice bath. Maintaining the cold bath, solid sodium bicarbonate was added to the stirring solution until the pH was neutral. The resulting product mixture was vacuum filtered to remove chromium precipitates. The filtrate was evaporated to dryness, dissolved in dichloromethane and any remaining water-soluble contaminents removed by water extraction in a separatory funnel. The bottom layer was collected and the solvent evaporated to dryness yielding an orange-brown solid (51%): ^{1}H NMR ($CDCl_3$) δ (ppm): 12.43-12.49 (1H, s, NH), 8.87 (1H, s, CH), 8.48 (1H, s, NH), 2.53 (3H, s, CH_3), 1.36 (9H, s, t-Bu). Anal. Calcd for C15H15N5O3.as a hemi-hydrate: C, 56.00; H, 5.00. Found: C, 56.37; H, 5.00. FT-IR (cm^{-1}): ν(N-H) 3246, 3198, 3111, ν(C≡C) 2202, ν(C=O) 1681, 1614, ν(C=N) 1546, 1474, 1436.

2-Pivaloyl-6-phenyl ethynyl pterin (PEPP). This procedure was followed as for BOPP using the following reagents: 2-pivaloyl-6-chloropterin (1.5g, 5.33 mmol), copper (I) iodide (0.136g, 0.714 mmol), palladium (II) acetate (0.16 g, 0.713 mmol), and 1,1'-bis(diphenylphosphino)-ferrocene (0.401 g, 0.723 mmol) were purged then dissolved in 40 mL of dried acetonitrile. Phenyl acetylene (1mL) and triethylamine (5mL) were added by syringe, the mixture stirred for 10 min at ambient temperature then heated at ~50 °C for 3 hours. Product isolation followed the procedure described for BOPP. The product was isolated as a cream solid (94%): ^{1}H NMR ($CDCl_3$) δ (ppm): 12.43-12.49 (1H, s, NH), 8.98 (1H, s, CH), 8.66 (1H, s, NH), 7.63-7.66 (2H, m, Ph) 7.41-7.46 (3H, m, Ph), 1.38 (9H, s, t-Bu). MS (HRESI) *m/z* 348.1451 (calcd for [M+H] C19H18O2N5 348.1460). FT-IR (cm^{-1}): ν(N-H) 3188, ν(C≡C) 2216, ν(C=O) 1680, 1618, ν(C=N) 1555, 1479, 1443.

2-Pivaloyl-6-(2,4-difluorophenyl) ethynyl pterin (DIFPEPP). This alkyne was prepared using the method for PEPP, substituting 2,4-difluorophenyl acetylene for phenyl acetylene in the procedure above.

Product purification and isolation was also accomplished as for PEPP. Anal. Calcd for C19H15N5O2F2 as hemihydrate: C, 58.16; H, 4.11. Found: C, 58.55; H, 3.84. MS (HRESI) *m/z* 384.1265 (calcd for [M+H] C19H16F2O2N5 384.1272) . ^{1}H NMR ($CDCl_3$) δ (ppm): 12.41 (1H, s, NH), 8.99 (1H, s, CH), 8.42 (1H, s, NH), 7.61 (1H, m, Ph) 6.93 (2H, m, Ph), 1.38 (9H, s, t-Bu). FT-IR (cm^{-1}): ν(N-H) 3158, ν(C≡C) 2220, ν(C=O) 1685, 1616, ν(C=N) 1552, 1513, 1481, 1438.

2-Pivaloyl-6-(3-hydroxy-3-methylbutyne)pterin (BMOPP). This procedure was followed as for BOPP using the following conditions: 2-pivaloyl-6-chloropterin (1.0000g, 3.55mmol), copper (I) iodide (0.095g, CuI), palladium (II) acetate (0.1015g, $Pd(OAc)_2$), 1,1-bis(diphenylphospino)ferrocene (0.254g) and dried acetonitrile (25 mL) was stirred at room temperature for approximately 10 minutes. 2-methyl-3-butyn-2-ol (3mL) and triethylamine (5mL) was added via syringe. The orange-yellow mixture was stirred and refluxed under nitrogen gas for 3 hours at 40-45 °C. The dark brown solution was cooled to room temperature, rotary evaporated to dryness then chromatographed on silica gel eluting the product with 5% MeOH/ CH_2Cl_2. A pale tan solid was obtained in 83% yield (0.9718g, 2.95mmol). MS (HRESI) *m/z* 330.1555 (calcd for [M+H] C16H20O3N5 330.1566) . ^{1}H NMR ($CDCl_3$) δ (ppm): 12.4 (s, 1H, NH); 8.9 (s, 1H, H7); 8.34 (s, 1H, NH); 2.1 (m, 1H, OH); 1.6 (d, 6H, CH_3); 1.3 (s, 9H, t-Bu). FT-IR (cm^{-1}): ν(O-H) 3470; ν(N-H) 3350, 3156; ν(C≡C) 2222, ν(C=O) 1682, 1612, ν(C=N) 1545, 1500, 1436.

[Et_4N][Tp*Mo^{IV}(S)S_4]. [Et_4N][Tp*$Mo(CO)_3$] (0.611 g, 1.01 mmol) and S_8 (0.265 g, 1.034 mmol) were dissolved in anhydrous dimethylformamide (15 mL). Basic alumina (0.70 g,), activated in a microwave oven immediately prior to use, was added to the reaction mixture. The contents were stirred at 25 °C for seven days under nitrogen atmosphere to produce a dark pine-green solution. The reaction solution was concentrated by evaporating DMF solvent under vacuum to approximately 5 mL. Precipitation was induced by addition of diethyl ether (50 mL). After chilling overnight at -30 °C, the dark green product was isolated by immersion filtration, washed several times with 20-30 mL diethylether and dried under nitrogen atmosphere. Yield: 0.657 g (96%). IR (KBr), cm^{-1}: ν(Mo=S), 470.41; ν(B-H), 2527.

[Et_4N][Tp*Mo^{IV}(O/S)S_2PEPP]. This procedure illustrates the synthesis using the mixed oxo/sulfido [Et_4N][Tp*Mo^{IV}(S/O)S_4] reagent. [Et_4N][Tp*Mo^{IV}(S/O)S_4] (0.450 g, 0.655 mmol) and PEPP (0.228 g, 0.657 mmol) were dissolved in CH_3CN (50 mL) and stirred at ~85 °C for 4 hours. The plum-brown colored reaction mixture was cooled to room temperature and stored below 0°C overnight to precipitate

any unreacted PEPP alkyne, which was subsequently removed by filtration. The solution was concentrated approximately to 5 mL by evaporating acetonitrile under vacuum then diethyl ether (50 mL) was added via syringe to precipitate a dark brown solid. The solid was isolated via immersion filtration and washed twice with diethyl ether (30 mL) and dried under nitrogen atmosphere to yield a dark brownish plum-colored solid as the crude product. Yield: 0.47 g (75%). FT-IR (KBr) cm^{-1}: ν(N-H) 3194, ν(B-H) 2523, ν(C=O) 1679, 1620, ν(Mo=O) 920, ν(Mo=S) 483. MS (HRESI) *m/z* 837.1609 (calcd for (M-H) 837.1519, M = C34H38O2N11S3BMo), 821.1759 (calcd for (M-H) 821.1756, M = C34H38O3N11S2BMo).

Tp*Mo^{V}(O)S$_2$PEPP was obtained by column chromatography of crude [Et$_4$N][Tp*Mo^{IV}(O/S)S$_2$PEPP] on silica gel under aerobic conditions, eluting with 5% methanol in dichloromethane. The amount of Tp*Mo^{V}(O)S$_2$PEPP isolated from the chromatographic purification is ~30 %. FT-IR (KBr) cm^{-1}: ν(N-H) 31942, ν(B-H) 2547, ν(C=O) 1687, 1617, ν(Mo=O) 929. MS (HRESI) *m/z* 821.1759 (calcd for (M - H) 821.1756, M = C34H38O3N11S2BMo).

[Et$_4$N][Tp*Mo^{IV}(S)S$_2$DIFPEPP]. This compound was prepared from [Et$_4$N][Tp*Mo^{IV}(S)S$_4$] (0.180 g, 0.25 mmol) and DIFPEPP (0.1108 g, 0.25 mmol) using the same procedure as for the preparation of [Et$_4$N][Tp*Mo^{IV}(S)S$_2$PEPP]. Yield: 0.224 g (89%). MS (HRESI) 873.1222 (calcd for (M - H) 873.1331, M = C34H36O2N11S3F2BMo); ESI-MS *m/z* 875 (M + H), 897 (M + Na), 1004 (M + TEA). FT-IR (KBr) cm-1: (Mo=S) 484.

[Et$_4$N][Tp*Mo^{IV}(O)S$_2$DIFPEPP]. Isolated crude product [Et$_4$N][Tp*Mo(S/O)S$_2$DIFPEPP] (0.110g, 0.110mmol) and triphenylphosphine (0.287g, 0.110mmol) were dissolved in a solution of wet acetonitrile (0.05% v/v H_2O/ CH_3CN 30mL) and stirred at ~70 °C under a nitrogen atmosphere for 4 hours. The dark brown colored reaction mixture was cooled to room temperature and concentrated to near dryness under vacuum. Diethyl ether (50mL) was added and mixture was stored below 0 °C for 3 days to complete precipitation. The supernatant was removed via immersion filtration to give a dark brown solid which was washed with diethyl ether (50 mL) and filtered, to produce a dark brown solid. Yield: 0.038g (38%). FT-IR (KBr) cm-1: (Mo=O) 922.

Tp*Mo^{V}(O)S$_2$DIFPEPP was obtained by column chromatography of crude product [Et$_4$N][Tp*Mo^{IV}(O/S)S$_2$DIFPEPP] on silica gel under aerobic conditions, eluting with 5% methanol in dichloromethane. Typical yield are ~ 35-40%. MS (HRESI) *m/z* 857.1663 (calcd for (M - H) 857.1568, M = C34H36O3N11S2F2BMo). FT-IR (KBr) cm-1: (N-H) 3201, (B-H) 2522, (C=O) 1679, 1619, (Mo=O) 931.

Mass Spectrometry. ESI-MS data were either obtained by Dr. Arpad Somogyi using a Finnigan LCQ HPLC/MS at the Mass Spectrometry Facility in the Department of Chemistry at the University of Arizona or using an Agilent LS-MS instrument at Haverford College, Haverford PA. High resolution ESI-MS (HRESI-MS) were obtained by Dr. Somogyi on an Ion Spec Fourier Transform Mass Spectrometer. Samples for mass spectral analysis were dissolved in acetonitrile under aerobic conditions and directly injected, bypassing the liquid chromatography column.

Magnetic Circular Dichroism Spectroscopy. Polymer thin film samples of Tp*Mo(5+)O(S$_2$DIFPEPP) and Tp*Mo(5+)O(S$_2$PEPP) were prepared for low-temperature magnetic circular dichroism spectroscopy (MCD) by dissolving the solid sample in a minimum amount of toluene and gently mixing this solution with a saturated solution of polystyrene in toluene until completely dissolved. This solution was then poured onto a flat glass plate and the solvent was allowed to slowly evaporate under a steady stream of N_2 in a glove bag. Polymer film samples were placed between two 1 mm Infrasil quartz disks housed in a custom designed sample cell.

Low-temperature MCD data were collected on an integrated MCD instrument employing track mounted Jasco J-810 (185 – 900 nm) and Jasco J-730 (700 - 2000 nm) spectropolarimeters which allow access to a single Oxford Instruments SM4000-7T superconducting magnetooptical cryostat (0-7 T, 1.4-300 K) employing an ITC503 Oxford Instruments temperature controller. All spectra were collected at a temperature of ~5 K in an applied magnetic field of 7.0 Tesla. The spectrometer was calibrated for circular dichroism intensity with camphorsulfonic acid, and the wavelength was calibrated using Nd-doped glass. Depolarization of the incident radiation by the sample was determined by comparing the intrinsic circular dichroism of a standard Ni (+)-tartrate solution positioned in front of and then in back of each sample. Samples which were <7% depolarized were deemed suitable.

Electron Paramagnetic Resonance Spectroscopy and Spectral Simulations. Solution and frozen glass

EPR spectra were measured at X-band (9.3 GHz) and Q-band (35 GHz) using a Bruker EMX spectrometer with associated Bruker magnet control electronics and microwave bridges. The room-temperature solution spectra were collected in toluene or dichloromethane solvent. For the low-temperature measurements, a 1:1 toluene-dichloromethane mixture was used as a glassing solvent, and the temperature was controlled using an Oxford Instruments liquid helium flow cryostat. Simulations of the EPR spectra were performed using the programs QPOW [29] or XSOPHE (Bruker).

Results and Discussion

Synthetic Method. The known reaction of transition metal sulfides and polysulfides with unsaturated carbon bonds serves as our entry into pterin-dithiolene ligand formation. Some examples of the fusion of Group VI metal sulfides with alkynes are illustrated in Figure 2.

Alkynes suitable for this coupling reaction, with only a few exceptions, must possess electron-withdrawing substituents for dithiolene formation on molybdenum and tungsten. The reactions in Fig. 2 show the use of alkynes substituted by carboxylate, acetyl, and polycyclic N-heterocycles [30].

Figure 2

We have synthesized several derivatives of alkynes substituted by pterin and these span a range of reactivities towards $Mo(S_4)$ moieties (Fig.3).

Figure. 3

Pterin Precursor Synthesis. The synthetic route to pterin-substituted alkynes proceeds through the regioselective preparation of 6-chloropterin developed by Taylor [39], the addition of a pivaloyl group at the 2-amino site to increase solubility, and a palladium catalyzed C-C coupling reaction to append the alkynyl unit (Fig. 4). This reaction sequence has been also used by other researchers, notably Joule [40], to form 2-alkynyl-quinoxaline compounds.

Figure 4

We have modified the C-C coupling method that produces the pterinyl alkynes BOPP and AEP from those first reported by Pilato et al. [35]. We find that the use of 1,1'-*bis*(diphenylphosphenyl)ferrocene

(DPPF) in place of tri-toluylphosphine (TTP) makes a significant improvement in the coupling reaction. Table 1 contrasts reactions conditions and pterinyl alkyne yields when DPPF instead of TTP is used.

Table 1

We have investigated reactions of the five alkynes AEP, BOPP, BMOPP, PEPP and DIFPEPP with two molybdenum tetrasulfide reagents, $[Tp^*Mo^{IV}(O/S)(S_4)]^-$ (this work) and $[Mo^{IV}O(S_4)_2]^{2-}$ (unpublished results). The pterinyl alkynes show a variety of reactivities towards these molybdenum tetrasulfide reagents where AEP and DIFPEPP react most readily and PEPP reacts most sluggishly in the formation of chelated pterin-dithiolene ligands.

Synthesis of oxo-Tp*Mo-*mono*-dithiolene compounds. The *tris*(3,5-dimethylpyrazolyl)borate ligand (Tp*) has been a successful framework on which to stabilize molybdenum and other metals enabling reactivity and spectroscopic studies focused on the remaining reactive coordination sites [41-42]. For this reason, the recently reported synthesis [43] of [TEA] $[Tp^*Mo^{IV}(O/S)(S_4)]$ (TEA = tetraethyl ammonium) was a welcome addition to the small number of molybdenum tetrasulfide reagents available for investigating reactions between alkynes and molybdenum polysulfides. The published procedure prepares $[TEA][Tp^*Mo^{IV}(O/S)(S_4)]$ from $[TEA][Tp^*Mo(CO)_3]$ reacted with elemental sulfur and reports that the reaction yields a 1:4 mixture of oxo- and sulfido species with the sulfido species in excess. The published report offered the speculation that the oxo species was formed as a result of trace moisture in the reaction. We have verified that deliberate addition of water to the reaction produces only $[TEA][Tp^*Mo(O)(S_4)]$ and no sulfido complex. Unfortunately, it is not possible to separate $[Tp^*Mo^{IV}(O)(S_4)]^-$ from $[Tp^*Mo^{IV}(S)(S_4)]^-$ by chromatography. Young and coworkers acquired pure $[Tp^*Mo^{IV}(S)(S_4)]^-$ through conversion of $[Tp^*Mo^{IV}(O)(S_4)]^-$ to $[Tp^*Mo^{IV}(S)(S_4)]^-$ by addition of boron sulfide [36]. We have found an alternate method to pure $[TEA][Tp^*Mo(S)(S_4)]$. The addition of basic alumina to the reaction of $[TEA][Tp^*Mo(CO)_3]$ and sulfur appears to adequately remove all water from the system to allow isolation of $[TEA][Tp^*Mo^{IV}(S)(S_4)]$ in high yields (>90%) uncontaminated by $[TEA][Tp^*Mo^{IV}(O)(S_4)]$.

The importance of producing pure $[TEA][Tp^*Mo^{IV}(S)(S_4)]$ is that only this species reacts with pterinyl alkynes in the coupling reaction to form pterin dithiolenes. When $[TEA][Tp^*Mo^{IV}(S)(S_4)]$ reacts with

either PEPP or DIFPEPP pteridinyl alkynes, a ~90% yield of plum-brown solid is obtained identified as the single species [TEA][Tp*Mo^{IV}(S)(S_2C_2(pterin)(R))] by ESI-MS, CV and FTIR (see below). The reaction using DIFPEPP alkyne is illustrated in Figure 5. In the circumstance where moisture has not been rigorously excluded, the oxo analog [TEA][Tp*Mo^{IV}(O)(S_2C_2(pterin)(R))] is also present in isolated product. Its identity is easily made through ESI-MS analysis of the product and its presence can be detected by cyclic voltammetry where an additional Mo(5+/4+) redox couple is observed. We note that Young et al. first made the observation that only the sulfido species [Tp*Mo(S)(S_4)]$^{-}$ reacts with activated alkynes during their investigations of dimethylacetylene carboxylate reactions with the mixed [TEA][Tp*Mo(O/S)(S_4)] which yields Tp*Mo(5+)(O)($S_2C_2(CO_2Me)_2$ (Fig. 2).

Column chromatography on silica accomplishes the separation of [Tp*Mo^{IV}(S)(S_2C_2(pterin)(R))]$^{-}$ and [Tp*Mo^{IV}(O)(S_2C_2(pterin)(R))]$^{-}$ from any other side products, however the Mo species isolated depends on whether chromatography is performed anaerobically or aerobically. Chromatography in air facilitates molybdenum oxidation and hydrolysis and is an effective means of converting a mixture of oxo- and sulfido-Mo(4+) dithiolene complexes to the reddish-brown oxo-Mo(5+)Tp*(dithiolene) complexes isolated in ~ 30% yield (Fig.5). Chromatography under a nitrogen atmosphere allows isolation of the sulfido-Mo(IV) dithiolene complexes albeit in a low < 25% yield with no contamination by oxo-Mo(4+) or -Mo(5+) species.

Product purification by column chromatography accomplishes conversion of the sulfido-Mo(4+) complexes to the oxo-Mo(5+) complexes, but is typically in low yield (~30%). We have investigated other direct means of hydrolyzing S=Mo(4+) to O=Mo(5+) complexes. Subjecting TEA[Tp*Mo(4+)(S)(S_2DIFPEPP)] to wet acetonitrile (0.5% v/v water) and mild heat (40-50 deg C) only partially hydrolyzes Mo=S to Mo=O. Addition of triphenylphosphine and heating at 60 deg is required to completely convert all sulfido groups to oxo ligands to produce Tp*Mo(5+)(O)(S_2DIFPEPP).

Figure 5

Pterin dithiolene synthesis using the two pterinyl-alkynes bearing hydroxyl-substituents, BOPP and BMOPP, are surprisingly complex. Preliminary results for the products observed by high resolution electrospray ionization mass spectrometry (HRESI-MS) include: (a) the initial product of BMOPP alkyne

coupling to the Mo-tetrasulfide is a tridithiolene species; (b) the pterin trithiolene complex can be converted to a pterin dithiolene complex through sulfur abstraction by PPh_3 , (c) dehydration of the hydroxyalkyl side chain occurs during silica gel chromatography. There is no indication of trithiolene complex formation in the aryl alkyne reactions of DIFPEPP and PEPP and therefore, at this time we do not know whether trithiolene precursors to dithiolenes are formed in every reaction of a pterinyl-alkyne and [TEA][Tp*Mo(S)(S_4)]. There is precedent for the formation of trithiolenes as the initial product of alkyne reaction with Mo(4+) tetrasulfide reagents [31]. The more complicated BOPP and BMOPP pterin-dithiolene model systems are still under study.

Attempts to adapt the alkyne-Mo(S_4) coupling methodology to prepare other Tp*Mo(O/S)(dithiolene) complexes from 2,4,-difluorophenyl ethyne or 2-pyridinylethyne showed that even under conditions a 20-fold excess of alkyne produces, only ~ 5% of the corresponding Tp*Mo(O)(S_2C_2(R)(H) (R-py, 2,4-difluorophenyl) formed. These low yields compared to those of pterin-dithiolene complexes obtained in 1:1 Mo/alkyne reaction stoichiometry underscores the importance of the electronic substituents on alkyne reactivity with Mo(S_4).

Prior to developing the pterin-dithiolene chemistry on the Tp*Mo scaffold, we attempted syntheses of oxo-Mo-*bis*(pterin-dithiolene) complexes through a similar synthetic strategy of reacting pterin alkynes with [TEA]$_2$[Mo(O)(S_4)$_2$]. The target compounds [TEA]$_2$[Mo(O)-*bis*(pterin-dithiolene)] formed were unstable towards dithiolene ligand dissociation and oxidation to pterin-thiophene compounds, a dithiolene ligand degradation reaction previously observed by us and others [32, 37]. The insurmountable problem of isolating purified materials for further studies led us to abandon this system of *bis*(pterin-dithiolene) complexes in favor of the robust [Tp*Mo(O/S)(pterin-dithiolene)] system. It is therefore important to note that we have not observed any tendency for the Tp*Mo(pterin-dithiolene) complexes to undergo oxidative dithiolene loss to form thiophenes, the problem plaguing our earlier attempts to prepare *bis*-dithiolene complexes. No thiophene decomposition products have been isolated during chromatography nor have been observed in ESI-MS analyses. The [Tp*Mo(5+)(X)(dithiolene)] complexes will be better suited for future exploration of redox manipulations of the pterin-dithiolene ligand.

Characterization of *mono*-pterin-dithiolene molybdenum complexes.

The new Tp*Mo-pterin-dithiolene compounds have been analyzed by high resolution electrospray ionization mass spectrometry (HRESI-MS), Fourier transform infrared spectroscopy (FTIR), cyclic voltammetry (CV), electron paramagnetic resonance (EPR) and magnetic circular dichroism (MCD). Product composition and purity is most easily afforded by a combination of ESI-MS and cyclic voltammetry analyses wherein all species can be detected. The purity of chromatographed samples of used in EPR and MCD experiments was verified by HRESI-MS and the data is shown in Fig. 6 for [Tp*Mo(O)(S_2DIFPEPP] and as supplementary data for [Tp*Mo(O)(S_2PEPP]. ^{1}H NMR spectra have been obtained for diamagnetic Mo(4+)-pterin-dithiolene compounds as crude products but these spectra are typically both complicated and of poor quality due to the mixture of Mo(4+) species and the presence of trace amounts of compounds isolated in the paramagnetic Mo(5+) state. Efforts to obtain crystals suitable for X-ray crystallography are underway but, to date, we have unfortunately been unsuccessful in growing crystals suitable for X-ray diffraction analysis.

Mass Spectrometry. Both 4+ and 5+ molybdenum pterin-dithiolene complexes are observed by ESI-MS. Mass spectra of neutral Mo(5+) complexes show signals as both [M + H] cationic adducts and as [M - H] anions after loss of a proton under the positive and negative polarization modes, respectively. Fig. 6 shows the HRESI spectra obtained from [Tp*Mo(O)(S_2DIFPEPP)] purified by aerobic chromatography where both the molecular anion $[M]^-$ and its doubly charged dianion $[M]^{2-}$ are observed for each complex in the full range spectra (A). (HRESI data for [Tp*Mo(O)(S_2PEPP)] is available as Supplemental Material.) The characteristic isotope pattern of the single prominent molybdenum species is enlarged in Fig. 6B to illustrate the match to the calculated mass spectra (Fig. 6C). The mono-anionic Mo(4+) pterin-dithiolene complexes isolated as [TEA]+ salts can be detected in the negative mode as [M-] anions (Fig. 7B) but are typically oxidized to Mo(5+) complexes during aerobic sample preparation and appear in the mass spectrum as both [M + H] and [M + TEA] cationic adducts, as illustrated for a sample of [TEA][Tp*Mo(4+)(S)(S_2DIFPEPP)] observed as the Mo(5+) species [M + H] in Fig. 7A. Since hydrolysis of the sulfido group, Mo=S, to an oxo group, Mo=O, occurs readily during MS sampling, the presence or absence of oxo species is best resolved by sample analysis by cyclic voltammetry, as discussed below.

Figure 6

Figure 7

Infrared Spectroscopy. Characteristic absorptions in the infrared due to the borohydride group, the Mo=O and Mo=S groups and the carbonyl moieties of the pterin were tracked during transformations during reactions and isolation procedures. Stretching vibrations of the Mo=O and Mo=S units are observed between 930-910 cm^{-1} and 495-480 cm^{-1} respectively, where the Mo(4+) complexes have frequencies at the lower end of the range (Table 2). The Mo(5+)=O vibration frequencies are very close to that reported for Tp*Mo(O)(S_2DMAC) [36]. The Mo(4+)=O/S vibration frequencies are at ~ 30 cm^{-1} lower energies compared to the related complexes Tp*Mo(4+)(O/S)(S_2CNR_2) complexes [44], probably due to the increased covalency and electronic delocalization afforded by the dithiolene over the dithiocarbamate chelate. The B-H stretching vibration is also a convenient diagnostic of the molybdenum oxidation state in these dithiolene complexes, where frequencies ~2545 and 2522 cm^{-1} correspond to the 5+ and 4+ state, respectively, and a similar range of values has been reported for Tp*Mo(=O/S) complexes bearing sulfur ligands [36, 38, 44, 47]. Little variation of the frequencies of pterin C=O and C=N modes is observed suggesting the pyrimidine ring of the pterin group is not much affected by electronic changes at the molybdenum and dithiolene.

Table 2

Cyclic Voltammetry. The new Tp*Mo-pterin-dithiolene model complexes exhibit reversible redox processes in the potential range between ~ 0 – -0.2 V (vs. Ag/AgCl) that are assigned to the Mo(5+/4+) redox couple and irreversible anodic processes between ~ 1.0 – 0.8 V (vs. Ag/AgCl) that are assigned to Mo(6+/5+) oxidation. Similar electrochemical behavior observed by CV has been reported for other Tp*Mo-oxo and -sulfido complexes bearing sulfur-donor ligands [36, 44, 45]. The irreversible Mo(5+)/(6+) oxidation indicates considerable instability of the Mo(6+) species, as is typically observed for other Tp*Mo systems [45]. Table 3 lists the reduction potentials for Mo(5+)/(4+) and Mo(6+)/(5+) couples for both the oxo- and the sulfido-dithiolene complexes in addition to reagents [TEA][Tp*MoO(S_4)] and [TEA][Tp*MoS(S_4)]. Data listed in Table 3 are reported vs the internal standard ferrocene/ferrocenium. The reduction of Mo(5+) to Mo(4+) in the sulfido complexes occurs at more negative potentials than for the corresponding oxo complexes and is ~150-200 mV more difficult to reduce. A similar ~200 mV difference between oxo- and sulfido- complexes of Tp*Mo(O/S)(S_2CNR_2) was also reported where the Mo(5+)=S was more difficult to reduce [44].

Table 3

Fig. 8 illustrates the usefulness of the CV technique for identification of sample composition. Multiple species observed in the crude product composed of [TEA][Tp*MoO(S_4)], [TEA][Tp*MoO(S_2DIFPEPP)] and [TEA][Tp*MoS(S_2DIFPEPP)] (Fig. 8A) can be distinguished by comparison with voltammagrams of purified [Tp*MoO(S_2DIFPEPP] (Fig. 8B), [TEA][Tp*MoS(S_2DIFPEPP)] (Fig. 8C) and [TEA][Tp*MoO(S_4)] (voltammogram not shown; data in Table 3).

Figure 8

CV can also reveal information about the chemical reactivity of species in solution. Fig. 9 provides an illustration where hydrolysis of the sulfido complex to form the oxo complex can be observed. In Fig. 9, a single reversible wave (a) is assigned as the Mo(5+)/(4+) couple of [Tp*Mo(S)(S_2DIFPEPP)]$^-$ when the potential sweep is limited to the +200 / -800 mV range. (This is the same process shown in Fig. 8C.) When the positive potential limit is increased to +1200 mV to allow observation of the Mo(6+)/(5+) process (c), the return sweep clearly shows formation of Tp*Mo(O)(S_2DIFPEPP) at wave (b). A side product of Mo=S hydrolysis is observed at -700 mV (d) and +0.6 mV.

Figure 9

The wealth of data available for Tp*Mo-oxo complexes allows an evaluation of the electronic effects of dithiolene substituents on Mo(5+/4+) reduction, especially the effect of oxidized pterin. This comparison is graphically depicted as an “electrochemical yardstick” in Figure 10. That the specific substituents on the dithiolene can have an enormous effect—almost 1 V—on the Mo reduction potential has been previously noted [15,47].

Figure 10

Spectroscopic Studies

Magnetic circular dichroism and EPR spectroscopies have been used to probe the ground and excited state electronic structure of [Tp*MoO(S_2PEPP)] and [Tp*MoO(S_2DIFPEPP)], since these are the best characterized of the *mono-* and *bis*-pterin-dithiolene complexes detailed in this study. Furthermore, detailed electronic absorption, MCD, and EPR studies have been performed on related oxomolybdenum mono-dithiolene complexes, and the new studies reported herein provide a context in which to interpret the effects of a pterin substituent on the electronic structure of the coordinated dithiolene in the enzymes [15,48-53].

EPR Spectroscopy. The room temperature isotropic solution X-band EPR spectra for [Tp*MoO(S_2DIFPEPP)] is shown in Figure 11; the isotropic EPR spectrum for [Tp*MoO(S_2PEPP)] is available as Supplemental Material. The spectra for [Tp*MoO(S_2DIFPEPP)] and [Tp*MoO(S_2PEPP)] are similar to one another and can be adequately simulated with g_{ave} = 1.976 and A_{iso} = 33.0 x10^{-4} cm^{-1} for [Tp*MoO(S_2PEPP)] and g_{ave} = 1.975 and A_{ave} = 33.4 x10^{-4} cm^{-1} for [Tp*MoO(S_2DIFPEPP)]. The isotropic EPR spin-Hamiltonian parameters for these compounds are very similar to those determined for [Tp*MoO(bdt)] (bdt = benzene-1,2-dithiolate), where g_{iso} = 1.971 and A_{iso} = 37 x10^{-4} cm^{-1} [**54**]. The larger g_{ave}/A_{iso} ratios for [Tp*MoO(S_2PEPP)] and [Tp*MoO(S_2DIFPEPP)] may be taken as an indication that the dithiolene sulfur atoms in these complexes are better donors in the Mo(V) oxidation state than those present in Tp*MoO(bdt) [55-56]. Unlike the other dithiolene ligands depicted in Figure 10, the aryl dithiolene substituents R in Tp*MoO(S_2PEPP) and Tp*MoO(S_2DIFPEPP) are not constrained with respected to rotation about the $C_{dithiolene}$-R bond. As such, variations in the π donor character of the coordinated dithiolene may be attenuated via rotation about the $C_{dithiolene}$-R bond as a function of oxidation state. This may explain why [Tp*MoO(S_2PEPP)] and [Tp*MoO(S_2DIFPEPP)] are easier to reduced than [Tp*MoO(bdt)], despite the larger g_{iso}/A_{iso} ratios for [Tp*MoO(S_2PEPP)] and [Tp*MoO(S_2DIFPEPP)].

Figure 11

The low-temperature anisotropic EPR spectra for [Tp*MoO(S_2DIFPEPP)] is presented in Figure 12 and that for [Tp*MoO(S_2PEPP)] is available as Supplemental Material. Since these oxomolybdenum dithiolenes possesses effective C_s symmetry, g_2 and A_2 are fixed by symmetry, corresponding to g_x and A_{xx} and aligned perpendicular to the mirror plane. This leaves g_3 (g_y) and A_3 (A_y) bisecting the dithiolene sulfur donors in the equatorial plane of the molecule. As anisotropic ^{95,97}Mo (I=5/2; 25.38% abundance) hyperfine parameters (A_{ii}) are often difficult to determine from solution spectral simulations, we have employed the approximation $A_{iso} \approx \langle A \rangle = (A_{xx}+A_{yy}+A_{zz})/3$, which relates the isotropic solution hyperfine parameter, $\langle A \rangle$, to A_{iso}. Low-symmetry oxo-molybdenum complexes are typically observed to display a noncoincidence of the **g** and **A**(^{95,97}Mo) tensors [57] where Euler angles are used to transform the **A**(^{95,97}Mo) hyperfine tensor onto that of the **g** frame. Although the model complexes considered in this study possess effective C_s symmetry, and are required to possess only one coincident set of principal **g** and **A**(^{95,97}Mo) axis, we have simulated the spectra assuming no Euler rotation. Therefore, the principal components of the **A**(^{95,97}Mo) tensors should be regarded as *effective* hyperfine parameters. It should be noted that there are inherent ambiguities associated with spectral simulations of frozen glass EPR spectra, and this underscores the need for detailed single crystal studies on oxomolybdenum *mono- and bis*-dithiolenes.

Figure 12

The anisotropic EPR spectra were analyzed using the spin-Hamiltonian given in Equation 1, where the parameters and symbols have their usual meaning.

$$\mathcal{H} = \beta H(g_{xx}\hat{S}_x + g_{yy}\hat{S}_y + g_{zz}\hat{S}_z) + A_{xx}\hat{S}_x\hat{I}_x + A_{yy}\hat{S}_y\hat{I}_y + A_{zz}\hat{S}_z\hat{I}_z \qquad (1)$$

Table 4

These spin-Hamiltonian parameters are presented in Table 4 along with those for *hpH* and *lpH* SO. A comparison of these results shows that the principal components of the **g** and **A**(^{95,97}Mo) tensors are remarkably similar for these model complexes, and this is somewhat surprising considering the fundamental differences in the dithiolene ligands. For these oxomolybdenum mono-dithiolenes, we have used an orthogonal right hand coordinate frame with the molecular *z* along the terminal oxo and *y* bisecting the two sulfur donors of the dithiolene. Thus, for [Tp*MoO(dithiolene)] the *x* axis is orthogonal to the mirror plane. Therefore, in this coordinate frame, g_1 and A_1 are colinear and tentatively assigned as g_z and A_z, closely aligned with the Mo=O bond [48, 57-61]. It has been shown that the principal factors which affect **g** tensor anisotropy for oxomolybdenum complexes are metal-ligand covalency, ligand spin-orbit coupling, and the presence of low energy L→Mo charge transfer states that mix into the ground state by the spin-orbit operator [58-60]. Thus, the similar **g** tensor components for Tp*MoO(S_2PEPP), Tp*MoO(S_2DIFPEPP), and Tp*MoO(bdt) point toward very similar Mo-S covalencies and charge transfer manifolds, indicating the MCD spectra should also be quite similar, *vide infra*.

MCD Spectroscopy. The 5K UV-Vis-NIR MCD spectra of [Tp*MoO(S_2PEPP)] and [Tp*MoO(S_2DIFPEPP)] are very similar and primarily composed of positive C-terms and an intense high energy pseudo A-term. The data for [Tp*MoO(S_2DIFPEPP)] are presented in Figure 13. Interestingly, the MCD bandshapes for [Tp*MoO(S_2PEPP)] and [Tp*MoO(S_2DIFPEPP)] are quite different from other oxomolydenum mono-dithiolenes, including [Tp*MoO(bdt)]. This is somewhat surprising in light of their very similar EPR spectra. Since the electronic absorption spectra for [Tp*MoO(S_2PEPP)] and [Tp*MoO(S_2DIFPEPP)] are complicated by intraligand transitions, we have Gaussian resolved the MCD spectrum of [Tp*MoO(S_2DIFPEPP)] using the minimum number of Gaussians necessary to reproduce the observed spectral features, keeping in mind that six transitions were assigned in the spectral region < ~25,000cm^{-1} for [Tp*MoO(bdt)] [49]. The band energies for [Tp*MoO(S_2DIFPEPP)] and [Tp*MoO(bdt)]are presented in Table 5. All of the bands below ~25,000cm^{-1} are positive C-terms which appear to

violate the MCD "sum rule"[63-64]. This indicates that there is extensive out-of-state spin orbit mixing of the low energy excited states with the ground state [63-64]. The most dominant feature of the spectrum is a large positive pseudo-A term, which is observed at 28,000 cm^{-1}.

Figure 13

Band Assignments. Due to the nearly identical EPR spectra and spin-Hamiltonian parameters for [Tp*MoO(S_2DIFPEPP)] and [Tp*MoO(bdt)], we have used the previous band assignments for [Tp*MoO(bdt)] as a guide for making tentative assignments for bands **1**-**6** in the MCD spectrum of [TpMoO(S_2DIFPEPP)] [49]. As in the case of the EPR analysis, we have assumed C_s symmetry in our MCD band assignments.

Band 1 is the lowest energy transition and can be assigned as the $\psi_{op}^{a'} \rightarrow \psi_{xy}^{a'}$ symmetric dithiolene out-of-plane to Mo(xy) LMCT transition while its partner, band 2, is assigned as the $\psi_{op}^{a''} \rightarrow \psi_{xy}^{a'}$ antisymmetric dithiolene out-of-plane to Mo(xy) LMCT transition (Fig. 14). Here, symmetric and antisymmetric refer to the phases of the two p_z orbital functions localized on the dithiolene sulfur atoms. These two transitions occur at an average energy that is ~1,700 cm^{-1} lower than the corresponding transitions for [Tp*MoO(bdt)]. Additionally, the transition energy differences between bands 1 and 2 are 4,250 cm^{-1} for [Tp*MoO(S_2DIFPEPP)] and 3,300 cm^{-1} for [Tp*MoO(bdt)]. Together, these data reflect the inherent energy differences between the S-C=C-S π systems of bdt and S_2DIFPEPP. Band 3 is observed at 15,800 cm^{-1} and is assigned as the $\psi_{xy}^{a'} \rightarrow \psi_{xz,yz}^{a'',a'}$ ligand field transition. The close similarity in ligand field transition energies for [Tp*MoO(S_2DIFPEPP)] and [Tp*MoO(bdt)] can be expected due to the identical first and second coordination sphere

Figure 14

Table 5

atoms in these molecules. It is anticipated that this ligand field transition should manifest itself as a pseudo A-term in the MCD spectrum of these complexes. However, this has not been experimentally observed and is likely a result of complications that arise from the low symmetry environment, low and inequivalent oscillator strengths for the individual $\psi_{xy}^{a'} \rightarrow \psi_{xz}^{a''}$ and $\psi_{xy}^{a'} \rightarrow \psi_{yz}^{a'}$ transitions, and out-of-state spin-orbit coupling [49]. Band 4 occurs at 17,600 cm^{-1}, approximately 1,700 cm^{-1} lower in energy than the

corresponding transition in [Tp*MoO(bdt)], where it has been assigned as the important $\psi_{ip}^{a'} \rightarrow \psi_{xy}^{a'}$ LMCT transition believed to probe the dominant hole superexchange pathway responsible for coupling the active sites of various pyranopterin Mo enzymes with endogenous and exogenous redox cofactors [49]. Band 5 has been assigned as a positive pseudo-A term at 21,000 cm^{-1} in [Tp*MoO(bdt)], but is observed as a positive C-term at 20,900 cm^{-1} in [Tp*MoO(S_2DIFPEPP)]. This transition in [Tp*MoO(S_2DIFPEPP)] is assigned as a single component of the $\psi_{op}^{a'} \rightarrow \psi_{xz,yz}^{a'',a'}$ LMCT band. Similarly, only a single component of the $\psi_{op}^{a''} \rightarrow \psi_{xz,yz}^{a'',a'}$ transition is observed in [Tp*MoO(S_2DIFPEPP)] at 25,100 cm^{-1}. This transition occurs at a similar energy for [Tp*MoO(bdt)], but both components of the transitions are observed as pseudo-A terms.

Conclusions

New models for the molybdenum cofactor incorporate the key structural feature found in all Mo and W enzymes, a dithiolene chelate appended by a pterin. The synthetic strategy builds the pterin-dithiolene ligand by coupling a Mo-tetrasulfide with a pterinyl alkyne to produce [Tp*Mo(O/S)(pterin-dithiolene)] complexes in both Mo(4+) and (5+) oxidation states. Described in this work is the characterization of the purified Mo(5+) species by electrochemistry, electron paramagnetic resonance and magnetic circular dichroism and preliminary studies on conversion of the Mo=S to a Mo=O. During the development of the Tp*Mo-pterin-dithiolene model complexes, improved syntheses of pterin alkynes and of [TEA][Tp*Mo(S)(S_4)] were accomplished. An important feature of these Tp*Mo-pterin-dithiolene models is that they are far more robust complexes that show none of the facile dithiolene loss and degradation that pervades molybdenum-*bis*(pterin-dithiolene) chemistry. Therefore, these models have great potential for studies of pterin redox chemistry possible for a pterin-substituted dithiolene ligand coordinated to Mo. It is expected that continued studies of these models whose electronic structure closely resembles that of the molybdenum active site will provide new spectroscopic and structural benchmarks to aid interpretation of analogous results from the enzymes and examples of fundamental chemistry needed to understanding the active site chemistry of Mo and W enzymes.

Acknowledgements

We are deeply appreciative of the inspiration and encouragement given freely and generously by Ed Stiefel and dedicate this work to his memory. Both SJNB and MLK are indebted to Ed Stiefel for his mentoring and continued support throughout their careers. SJNB is also grateful for the synthetic

expertise of co-workers Wendy Belliston, Susan Ashton, Francine Morris, Ria Sankar and Mica Grantham who contributed to the development of this work. Funding to SJNB for a portion of this work was from NIH-AREA (GM60264-01) and NSF-9973673. M.L.K. gratefully acknowledges financial support from the National Institutes of Health (GM-057378) for support of this work.

References

[1] E. I. Stiefel, Met. Ions in Biol. Sys. 39 (2002) 1-29.

[2] R. S. Pilato, E. I. Stiefel, in: J. Reedjik (Ed) Bioinorganic Catalysis: Molybdenum and Tungsten Enzymes. (1999) Dekker, New York, pp 81-152.

[3] E. I. Stiefel, Science Spectra 7 (1996) 62-67.

[4] E. I. Stiefel, Science 272 (1996) 1599-1600.

[5] R. R. Mendel, Planta 203 (1997) 399-405.

[6] R. R. Mendel, G. Schwarz, Crit. Rev. Plant Sci. 18 (1999) 33-69.

[7] J. Kuper, T. Palmer, R. R. Mendel, G. Schwarz, Proc. Natl. Acad. Sci. USA 97 (2000) 6475-6480.

[8] G. Schwarz, R. R. Mendel, Ann. Rev. Plant Biol. 57 (2006) 623-647.

[9] C. Mize, J. L. Johnson, K.V. Rajagopalan, J. Inher. Met. Disease 18 (1995) 283-90.

[10] E. Karakas, H. L. Wilson, T N. Graf, S. Xiang, S. Jaramillo-Busquets, K. V. Rajagopalan, J. Biol. Chem. 280 (2005) 33506-33515.

[11] S. Leimkuehler, A. Freuer, J.A. S. Araujo, K. V. Rajagopalan, R. R. Mendel, J. Biol. Chem 278 (2003) 26127-26134.

[12] J. L. Johnson, K.E. Coyne, R. M. Garrett, M-T. Zabot, C. Dorche, C. Kisker, K.V. Rajagopalan, Human Mutation 20 (2002) 1-6.

[13] H. Schindlin, C. Kisker, J. Hilton, K.V. Rajagopalan, D.C. Rees, Science 272 (1996) 1615-1521.

[14] S. J. N. Burgmayer, Prog. Inorg. Chem. 52 (2004) 491-538.

[15] M. L. Kirk, M. E. Helton, R. L. McNaughton, Prog. Inorg. Chem. 52 (2004) 111-212.

[16] B. L. Westcott, N. E. Gruhn, J. H. Enemark, J. Am. Chem. Soc. 120 (1998) 3382-3386.

[17] R. L. Mcnaughton, M. E. Helton, N. D. Rubie, M. L. Kirk *Inorg. Chem.* 39 (2000) 4386-4387.

[18] B. S. Lim, M. W. Willer, M. Miao, R. H. Holm, J. Am. Chem. Soc. 123 (2001) 8343-8349.

[19] B. Lim, R. H. Holm, J. Am. Chem. Soc. 123 (2001) 1920-1930.

[20] S. J. N. Burgmayer, D. L. Pearsall, S. Blaney, E. Moore, C. Sauk-Schubert,
C. J. Biol. Inorg. Chem. 9 (2004) 59-63.

[21] S. J. N. Burgmayer, M. A. Arkin, L. Bostick, S. Dempster, K. M. Everett, H. Layton, K. Paul, C. Rogge, J. Am. Chem. Soc. 117 (1995) 5812-5823.
[22] H. L. Kaufmann, L. Liable-Sands, A. L. Rheingold, S. J. N. Burgmayer, Inorg. Chem. 38 (1999) 2592-2599.
[23] H. L. Kaufmann, P. J. Carroll, S. J. N. Burgmayer, Inorg. Chem. 38 (1999) 2600-2606.
[24] S. J. N. Burgmayer, H. L. Kaufmann, G. Fortunato, P. Hug, B. Fischer, Inorg. Chem. 28 (1999) 2607-2612.
[25] B. Fischer; J. Strahle; M. Viscontini. Helv. Chim. Acta 74 (1991) 1544-1547.
[26] J. P. McNamara, J. A. Joule, I. H. Hillier, C. D. Garner, Chem. Comm. 2 (2005) 177-179.
[27] M. G. Bertero, R. A. Rothery, M. Palak, D. Lim, F. Blasco, J. H. Weiner, N. C. Strynadka, Nat. Struct. Biol. 10 (2003) 681-687.
[28] M. D. Curtis, K. Shiu, Inorg. Chem. 24 (1985) 1213-1218.
[29] M. J. Nilges, 1979. Electron Paramagnetic Resonance Studies of Low Symmetry Nickel(I) and Molybdenum(V) Complexes. Ph.D. dissertation, University of Illinois, Urbana, IL.
[30] T. B. Rauchfuss, Prog. Inorg. Chem. 52 (2004) 1-54.
[31] D. Coucouvanis, A. Hadjikyiacou, M. Dragajac, M. G. Kanatzidis, O. Ileperuma, Polyhedron 5 (1986) 349-356.
[32] C. L. Soricelli, V. A. Szalai, S. J. N. Burgmayer, J. Am. Chem. Soc. 113 (1991) 9877-9878.
[33] D. Coucouvanis, A. Hadjikyiacou, A. Toupadakis, S.-M. Koo, O. Ileperuma, M. Dragajac, A. Salioglou, Inorg. Chem. 30 (1991) 754-.
[34] M. A. Ansari, J. Chandrasekaran, S. Sarkar, Inorg. Chim. Acta 133 (1987) 133-136.
[35] R. S. Pilato, K. A. Eriksen, M. A. Greaney, E. I. Stiefel, S. Goswami, L. Kilpatrick, T. G. Spiro, E. C. Taylor, A. L. Rheingold, J. Am. Chem. Soc. 113 (1991) 9372-9374.
[36] S. A. Sproules, H. T. Morgan, C. J. Doonan, J. M. White, C. G. Young, C. G. Dalton Trans. (2005) 3552-3557.
[37] A. A. Eagle, G. N. George, E. R. T. Tiekink, C. G. Young, J. Inorg. Biochem. 76 (1999) 39-45.
[38] P.J. Lim, D. A. Slizys, E. R. T. Tiekink, C. G. Young, Inorg. Chem. 44 (2005) 114-121.
[39] E. C. Taylor, P.S. Partha, J. Org. Chem. 52 (1987) 3997-4000
[40] B. Bradshaw, A. Dinsmore, D. Collison, C. D. Garner, J. A. Joule, J. Chem. Soc., Perkin Trans. 1 (2001) 3232-3238.
[41] J. H. Enemark, J. J. A. Cooney, J. –J. Wang, R. H. Holm, Chem. Rev. 104 (2004) 1175–1200.
[42] C. G. Young, J. Biol. Inorg. Chem. 2 (1997) 810-816.

[43]H. Seino, Y. Arai, N. Iwata, S. Nagao, Y. Mizobe, M. Hidai, Inorg. Chem. 40 (2001)1677–1682.
[44] C. G. Young, S. A. Roberts, R. B. Ortega, J. H. Enemark, J. Am. Chem. Soc. 109 (1987) 2938-2946.
[45] W. E. Cleland, K. M Barnhart, K. Yamanouchi, D. Collison, F.E. Mabbs, R. B. Ortega, J. H. Enemark, Inorg. Chem. 26 (1987) 1017-1025.
[46] C-S. J. Cheng, J. H. Enemark, Inorg. Chem. 30 (1991) 683-688.
[47] M. E. Helton, N. E. Gruhn, R. L. Mcnaughton, M. L. Kirk, Inorg. Chem. 39 (2000) 2273-2278.
[48] M. L. Kirk, K. Peariso, Polyhedron 23 (2004) 499-506.
[49] F. E. Inscore, R. L. McNaughton, B. L. Westcott, M. E. Helton, R. Jones, I. K. Dhawan,J.H. Enemark, M. L. Kirk, Inorg. Chem. 38 (1999) 1401-1410.
[50] M. D. Carducci, C. Brown, E. I. Solomon, J. H. Enemark, J. Am. Chem. Soc. 116 (1994) 11856-11868.
[51] M. E. Helton, N. L. Gebhart,E. S. Davies, J. McMaster, C. D. Garner, M. L. Kirk, J. Am. Chem. Soc. 23 (2001) 10389-10390.
[52] M. E. Helton, R. L. McNaughton, M. L. Kirk, Abst. Am. Chem. Soc. 217 (1999) U1085.
[53] M. E. Helton,A. Pacheco, J. McMaster, J. H. Enemark, M. L. Kirk, J. Inorg. Biochem. 80 (2000) 227.
[54] I. Dhawan, J. H. Enemark, Inorg. Chem. 35 (1996) 4873-4882.
[55] W. E. Cleland, K. M. Barnhart, K. Yamanouchi, D. Collison, F. E. Mabbs, R. B. Ortega, J. H. Enemark, Inorg. Chem. *26* (1987) 1017-1025.
[56] D. Collison, F. E. Mabbs, J. H. Enemark, W. E. Cleland, Polyhedron 5 (1986) 423-425.
[57] M. M. Cosper, F. Neese, A. V. Astashkin, M. Carducci, A. M. Raitsimring, J. H. Enemark, Inorg. Chem. 44 (2005) 1290-1301.
[58] C. Balagopalakrishna, J. T. Kimbrough, T. D. Westmoreland, Inorg. Chem. 35 (1996) 7758-7768.
[59] N. S. Nipales, T. D. Westmoreland, Inorg. Chem. 36 (1997) 756-757.
[60] J. Swann, T. D. Westmoreland, Inorg. Chem. 36 (1997) 5348-5357.
[61] K. Peariso, B. S. Chohan, C. J. Carrano, M. L. Kirk, Inorg. Chem. 42 (2003) 6194-6203.
[62] I. K. Dhawan, J. H. Enemark, Inorg. Chem. 35 (1996) 4873-4882.
[63] M. L. Kirk, K. Peariso, K. Curr. Op. Chem. Biol. 7 (2003) 220-227.
[64] F. Neese, E. I. Solomon, Inorg. Chem. 38 (1999) 1847-1865.

Table 1. Comparative Reaction Conditions and % Yields of Pterinyl Alkynes

Alkyne	**P(aryl)$_3$**	**reaction conditions**	**% yield**
BOPP	$P(Ph)_3$	8 h, 60 deg C	no reaction
	$P(tol)_3$	8 h, 60 deg C	60%
	DPPF	3 h, 40 deg C	88%
PEPP	$P(tol)_3$	8 h, 80 deg C	44%
	DPPF	4.5 h, 40 deg C	78%
DIFPEPP	DPPF	4.5 h, 40 deg C	90%

Table 2. Infrared Data for Tp*MoX(pterin-dithiolene) complexes

Tp*MoX(dithiolene)			$\nu_{Mo=O}$	$\nu_{Mo=S}$	ν_{B-H}	$\nu_{C=O}$
Mo	X	dithiolene				
+5	O	S_2PEPP	929	---	2545	1719sh[a], 1685, 1619
+5	S	S_2PEPP	---	493	2546	1719sh, 1683, 1618
+4	S	S_2PEPP	---	483	2523	1719sh, 1685, 1620
+5	O	S_2DIFPEPP	929	---	2545	1720sh, 1683, 1616
+4	O	S_2DIFPEPP	922	---	2522	1719sh, 1685, 1617
+5	S	S_2DIFPEPP	---	493	2545	1720sh, 1683, 1616
+4	S	S_2DIFPEPP	---	484	2522	1717sh, 1675, 1620

[a] shoulder

Table 3. Electrochemical data for oxo- and sulfido-molybdenum pterin-dithiolene compounds and the molybdenum tetrasulfide precursors.

	$E\ (Mo^{5/4})$	ΔE_{pp}	i_a / i_c	$E\ (Mo^{6/5})$	ΔE_{pp}	i_a / i_c
$[Tp^*Mo^{4+}O(S_4)]^-$	E_a = -0.20	----	Irr.	+0.56	70	0.93
$[Tp^*Mo^{4+}S(S_4)]^-$	E_a = -0.36	----	Irr.	----	----	----
$[Tp^*MoO(S_2DIFPEPP)]$	-0.44	70	0.93	+0.45	70	1.4
$[Tp^*MoS(S_2DIFPEPP)]$	-0.58	60	0.97	----	----	----
$[Tp^*MoO(S_2PEPP)]$	-0.43	68	1.0	+0.54	68	v.irr.
$[Tp^*MoS(S_2PEPP)]$	-0.59	78	1.0			
$[Tp^*MoO(S_2DMAC)]$[a]	-0.35 (ACN); -0.461 (DCE)	68	1.0	----	----	----

All potentials referenced to internal ferrocene whose potential is +0.40 vs. a Ag/AgCl reference electrode. ACN, acetonitrile; DCE, 1,2 dichloroethane; ---- indicates redox couple was not observed.

[a] This compound was prepared according to Sproules et al. [36]. Electrochemical results agree with those reported in ACN.

Table 4. EPR Parameters for sulfite oxidase and some oxo-molybdenum(V) models[a].

Sample	g_1	g_2	g_3	<g>[b]	A_1	A_2	A_3	<A>[b]	α[c]	β[c]	γ[c]	Ref.
hpH SO	1.990	1.966	1.954	1.970	54.4	21.0	11.3	28.9	0	14	22	62
lpH SO	2.007	1.974	1.968	1.983	56.7	25.0	16.7	32.8	0	18	0	62
Tp*MoO(S_2PEPP)	2.006	1.976	1.936	1.973	46.7	3.3	50.4	33.5	0	0	0	d
Tp*MoO(S_2DIFPEPP)	2.006	1.976	1.936	1.973	47.3	3.3	51.0	33.9	0	0	0	d
Tp*MoO(bdt)	2.004	1.972	1.934	1.971	50.0	11.4	49.7	37.0	0	0	0	62

a. A(^{95,97}Mo) are reported x10^{-4} cm^{-1}.

b. <g> and <A> are the average g and A values, calculated as $\frac{1}{3}(X_1 + X_2 + X_3)$. (see F.E. Mabbs and D. Collison in "Electron Paramagnetic Resonance of d Transition Metal Compounds", Elsevier, 1992, p. 126).

c. α, β, and γ are the Euler angles that relate the orientation of the principal axes of the A tensor onto those of the g tensor.

d. This work

Table 5. MCD Spectral Parameters[a]

	Tp*MoO(bdt)		Tp*MoO(S_2DIFPEPP)	
	$E^{(MCD)}$ cm^{-1}	Assignment and MCD term	$E^{(MCD)}$ cm^{-1}	Assignment and MCD term
Band 1	9 100	$\psi_{op}^{a'} \rightarrow \psi_{xy}^{a'}$ +C	6 950	$\psi_{op}^{a'} \rightarrow \psi_{xy}^{a'}$ +C
Band 2	12 400	$\psi_{op}^{a''} \rightarrow \psi_{xy}^{a'}$ -C	11 200	$\psi_{op}^{a''} \rightarrow \psi_{xy}^{a'}$ +C
Band 3	15 700	$\psi_{xy}^{a'} \rightarrow \psi_{xz,yz}^{a'',a'}$ +C	15 800	$\psi_{xy}^{a'} \rightarrow \psi_{xz,yz}^{a'',a'}$ +C
Band 4	19 300	$\psi_{ip}^{a'} \rightarrow \psi_{xy}^{a'}$ +C	17 600	$\psi_{ip}^{a'} \rightarrow \psi_{xy}^{a'}$ +C
Band 5	21 000	$\psi_{op}^{a'} \rightarrow \psi_{xz,yz}^{a'',a'}$ +pseudo A	20 900	$\psi_{op}^{a'} \rightarrow \psi_{xz,yz}^{a'',a'}$ +C
Band 6	24 600	$\psi_{op}^{a''} \rightarrow \psi_{xz,yz}^{a'',a'}$ +pseudo A	25 100	$\psi_{op}^{a''} \rightarrow \psi_{xz,yz}^{a'',a'}$ +C

[a]A positive pseudo A-term is a derivative shaped MCD feature with the positive component at higher energy. E^{max} represents the maximum in C-term intensity, or the point at which the pseudo A-term changes sign.

Figure Legends

Figure 1. The structure of the pyranopterin dithiolene chelate found uniquely in Mo and W enzymes. Many bacterial enzymes have the additional feature of a nucleotide appended at the phosphate.

Figure 2. Examples of dithiolene ligand formation from reactions of molybdenum and tungsten sulfides and polysulfides with alkyne reagents.

Figure 3. Pterinyl alkynes prepared in this work and their designated abbreviations.

Figure 4. Synthetic route to pterinyl alkynes. (i) pivaloylanhydride; (ii) DFFP, CuI, $Pd(acetate)_2$; (iii) CrO_3/H_2SO_4.

Figure 5. Synthetic route to [Tp*Mo(5+)(O)(S_2C_2(pterin)(R))] complexes as illustrated for the pterinyl alkyne DIFPEPP forming [TEA][Tp*Mo(4+)(S)(S_2DIFPEPP)] and [Tp*Mo(5+)O(S_2DIFPEPP)].

Figure 6. HRESI-MS of [Tp*MoO(S_2DIFPEPP)]. **A**: full spectrum within range *m/z* 200-2000 where both the molecular anion $[M]^-$ and its doubly charged dianion $[M]^{2-}$ are observed at *m/z* 857.1663 and 428.5785, respectively; **B**: enlarged signal showing isotopic distribution in the molecular anion $[M]^-$; **C**: calculated mass spectrum for the molecular anion $[M]^-$.

Figure 7. ESI-MS. **A**: spectrum from dissolution of [TEA][Tp*Mo(4+)(S)(S_2DIFPEPP)] in acetonitrile to show its detection as the Mo(5+) species as a [M + H] cation adduct at *m/z* 875; **B:** spectrum from a sample mixture of [TEA][Tp*Mo(O/S)(S_2DIFPEPP)] showing detection of each species, oxo and sulfido complexes, as the [M] anions at *m/z* 857 and 873, respectively.

Figure 8. Cyclic voltammagrams of Tp*Mo(O/S)(S_2DIFPEPP) products analyzed in 0.10M TEAP in acetonitrile using a Pt disk working electrode, Pt wire auxiliary electrode, and Ag/AgCl reference electrode using a scan rate of 100 mV/sec where the plot potentials are referenced to Ag/AgCl. The scan began at the negative potential limit. **A**: the crude product showing the mixture of unreacted $[Tp*Mo^{4+}O(S_4)]^-$, $[Tp*MoO(S_2DIFPEPP)]^-$ and $[Tp*MoS(S_2DIFPEPP)]^-$; **B:** Tp*MoO(S_2DIFPEPP)

isolated from chromatography; **C**: [TpMoS(S_2DIFPEPP)]$^-$ isolated from synthesis with pure [TEA][Tp*MoS(S_4)]$^-$. The assignments of the various couples are: (a) Mo(5+/4+) of [Tp*MoS(S_2DIFPEPP)]$^-$; (b) Mo(5+/4+) of [Tp*MoO(S_2DIFPEPP)]$^-$: (c) Mo(5+/4+) of unreacted [Tp*MoO(S_4)]$^-$: (d) overlapping Mo(6+/5+) processes due to all Tp*MoO species present and (e) Mo(6+/5+) of [Tp*MoO(S_2DIFPEPP)]$^-$

Figure 9. Cyclic voltammogram illustrating the reversible Mo(5+/4+) reduction (a) and irreversible Mo(6+/5+) oxidation (c) in [TEA][Tp*MoS(S_2DIFPEPP)]. The plot potentials are plotted vs the Ag/AgCl reference electrode. The cathodic peak at (b) is the reduction of [Tp*Mo(5+)O(S_2DIFPEPP)] formed in situ when the scanned through +1.2 V. The peak at (d) and at +0.6 mV correspond to an unknown product of S=Mo hydrolysis. The pseudo-irreversible peak (e) at +0.24 V is a small amount of unreacted [Tp*MoO(S_4)]$^-$. The initial scan begins at the * and scans to –0.9 V then continues cycling through +1.2 V. Conditions: 0.10M TEAP in acetonitrile, Pt disk working electrode, Pt wire auxiliary electrode, Ag/AgCl reference electrode; potentials shown are referenced to Ag/AgCl using a scan rate of 100 mV/sec.

Figure 10. A Mo(5+/4+) reduction "yardstick" showing the relative electronic effect of pterin substituents on chelating dithiolene ligands in comparison with chelating *bis*-dithiolates and thiolates in Tp*Mo(=O)(S-S) complexes. Potentials are referenced vs. Ag/AgCl in acetonitrile. All potentials were measured in this work, except for ligands –SPh, -SEt, ead and 2,3-butenedithiolate whose values have been reported in the literature [45, 46].

Figure 11. Room temperature solution EPR spectrum of [Tp*MoO(S_2DIFPEPP)] (red) and spectral simulation (blue).

Figure 12. Low temperature frozen glass EPR spectrum of [Tp*MoO(S_2DIFPEPP)] (red) and spectral simulation (blue).

Figure 13. Low temperature (5K) MCD spectrum of [Tp*MoO(S_2DIFPEPP)] (red). Gaussian resolved bands are presented as dashed lines and the resultant spectral simulation is given in blue.

Figure 14. Left: Approximate energy level diagram for Mo d and dithiolene orbitals. Upper right: Coordinate frame for [Tp*MoO(dithiolene)]. Lower right: Symmetry adapted linear combinations of ditiolene S(p) orbitals.

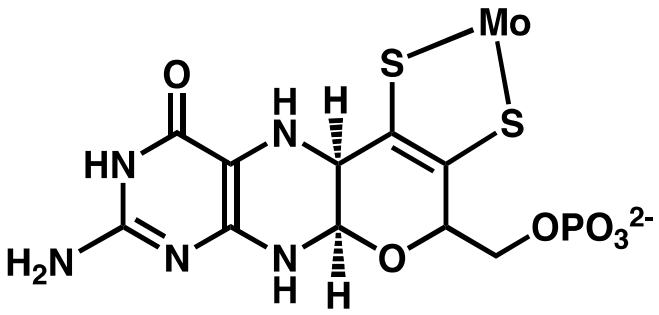

Figure 1

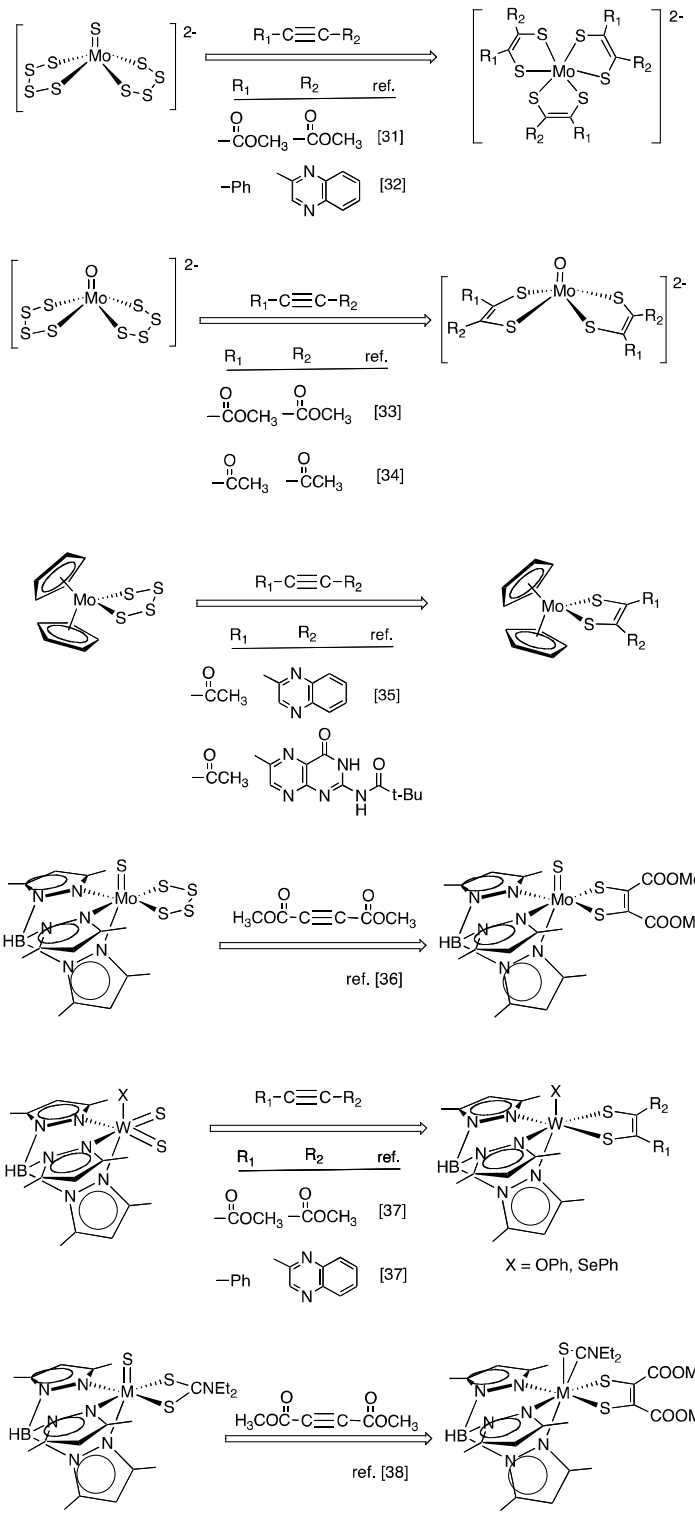
R1–C≡C–R2
R1 R2 ref.
[31]
–Ph
[32]
[33]
[34]
[35]
ref. [36]
ref. [37]
X = OPh, SePh
M = Mo, W
ref. [38]

Figure 2

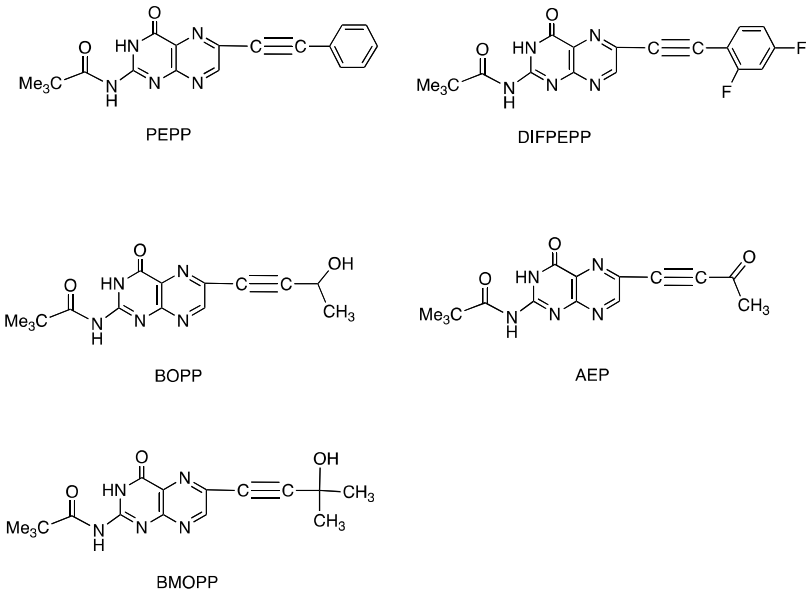

Figure 3

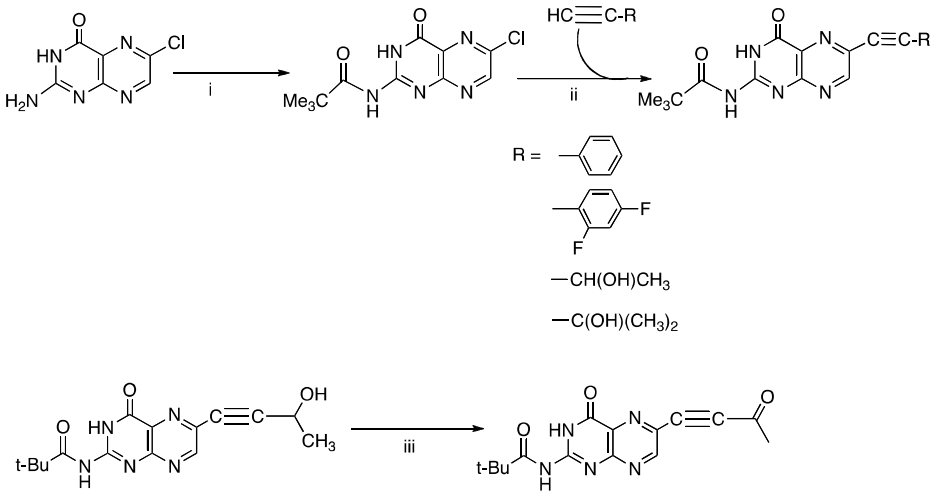

Figure 4

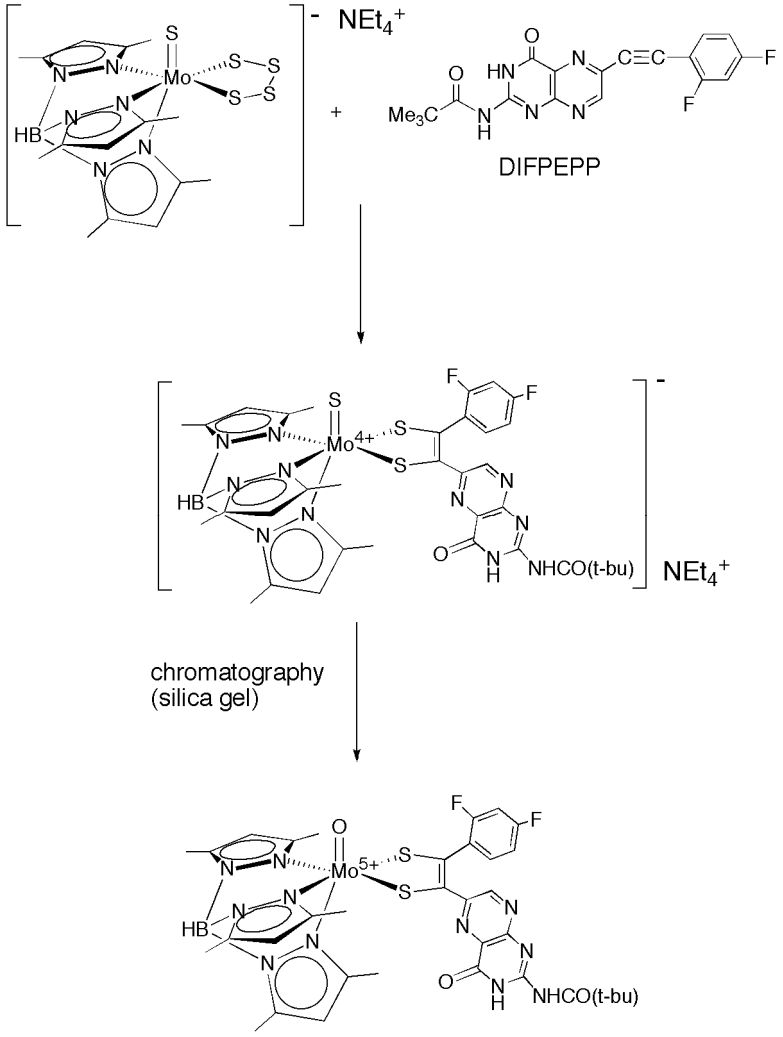
NEt4+
DIFPEPP
chromatography
(silica gel)
NHCO(t-bu)
NEt4+
NHCO(t-bu)

Figure 5

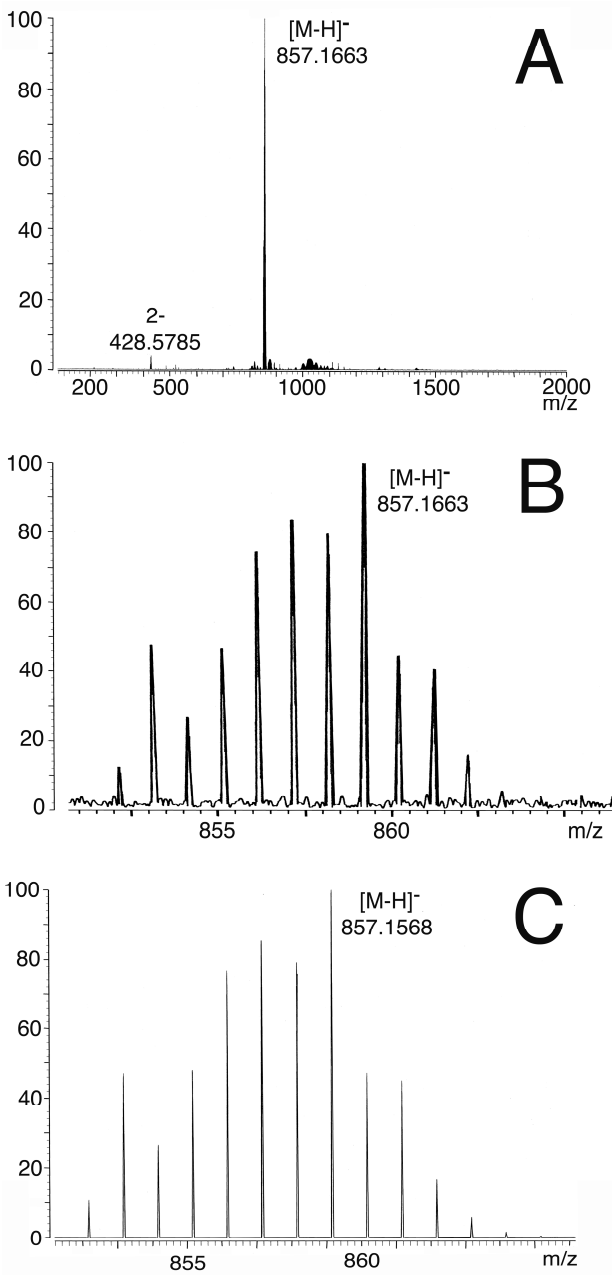
A
[M-H]-
857.1663
2-
428.5785
100
80
60
40
20
0
200
500
1000
1500
2000
m/z
B
[M-H]-
857.1663
855
860
m/z
C
[M-H]-
857.1568
855
860
m/z

Figure 6

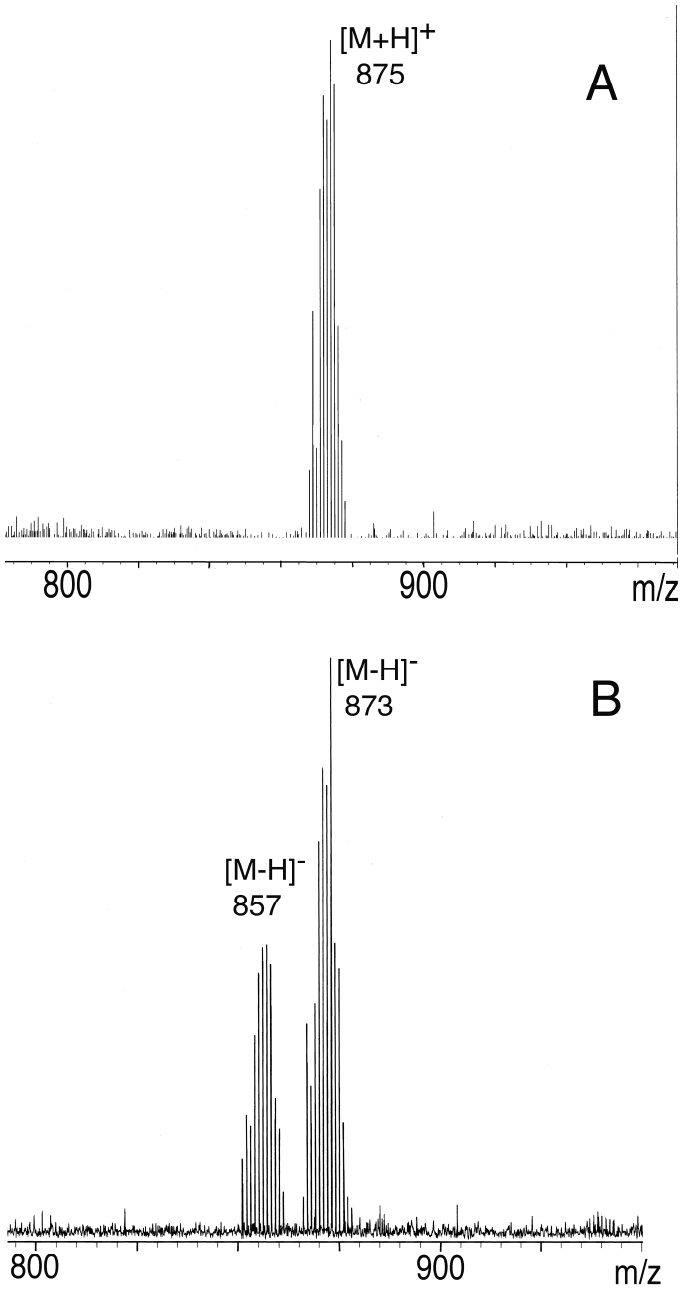

Figure 7

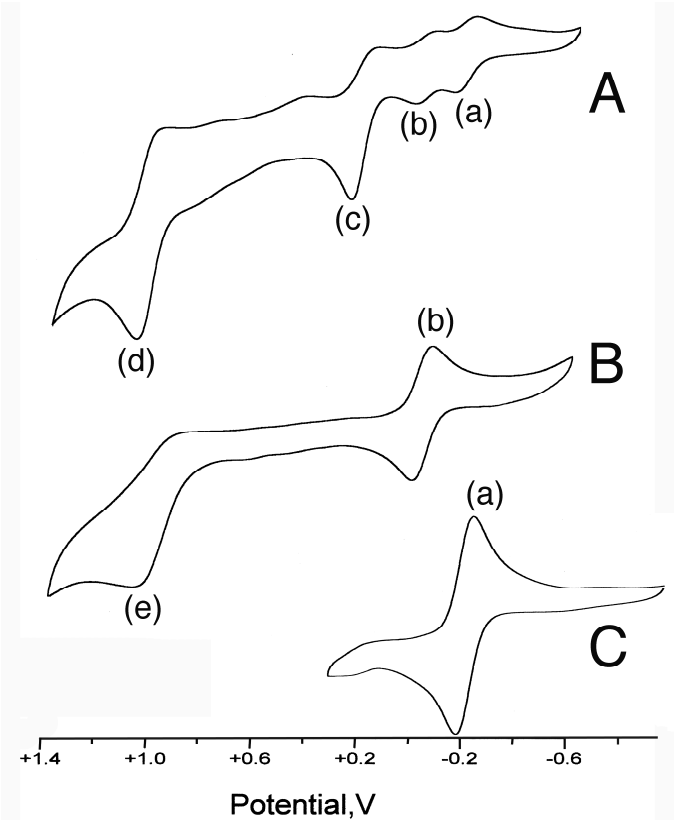

Figure 8

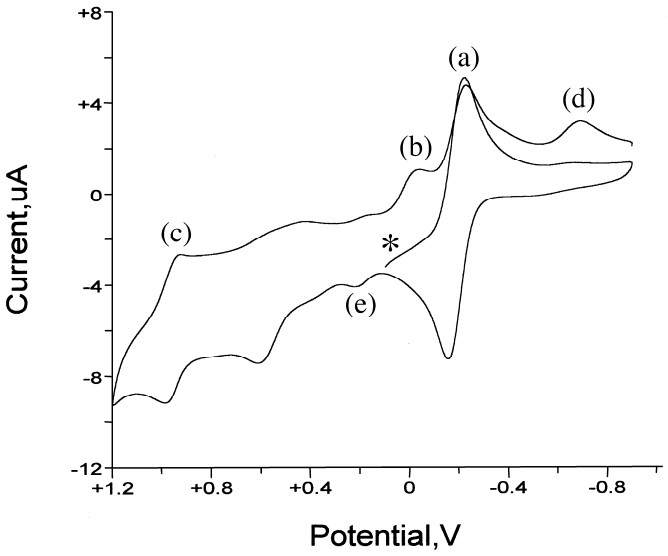

Figure 9

Figure 10

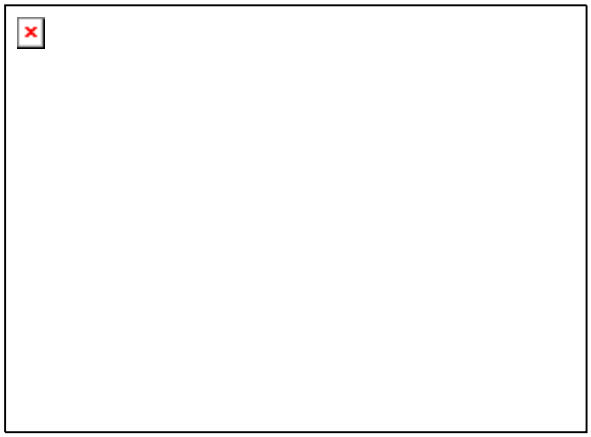

Figure 11 (color for on-line publication)

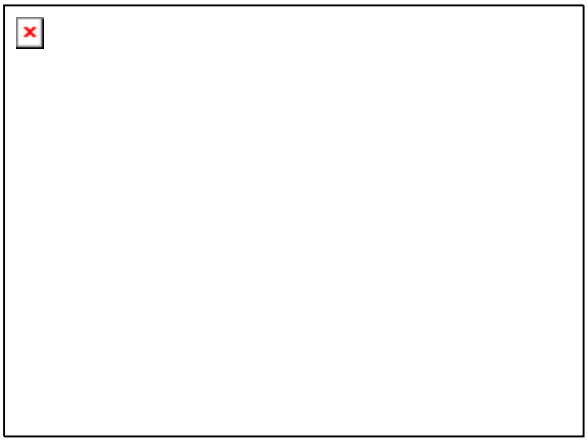

Figure 11 (BW for print publication)

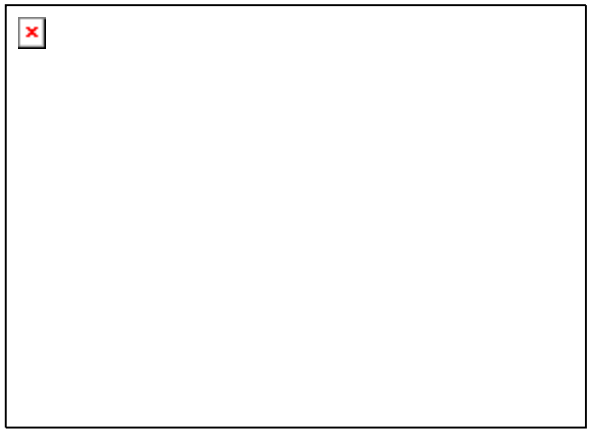

Figure 12 (color for on-line publication)

Figure 12 (BW for print publication)

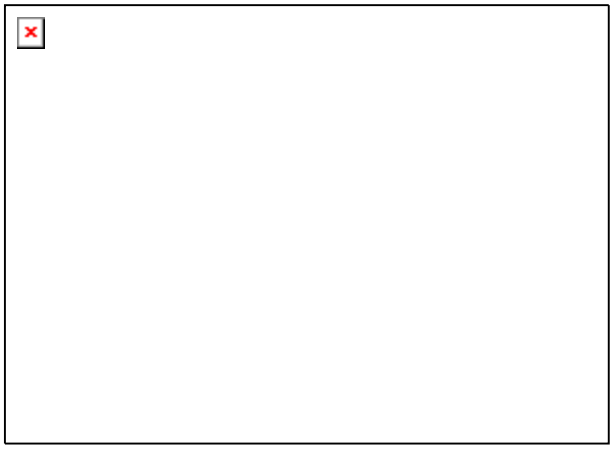

Figure 13

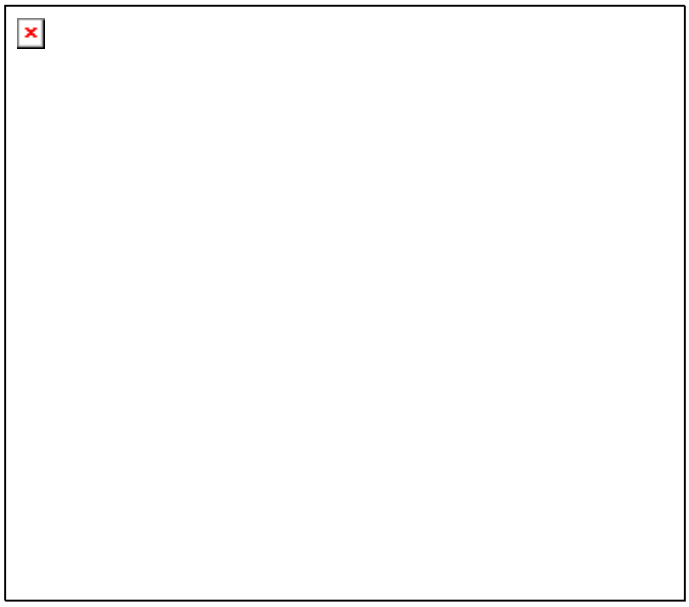

Figure 14

Supplemental Material Headings

S1. HRESI-MS of [Tp*MoO(S_2PEPP)]. **A**: full spectrum within range *m/z* 200-2000 where both the molecular anion $[M]^-$ and its doubly charged dianion $[M]^{2-}$ are observed at *m/z* 819.1759 and 410.5930, respectively; **B**: enlarged signal showing isotopic distribution in the cationic adduct [M+H]; **C**: calculated mass spectrum for the cationic adduct [M+H].

S2. Room temperature solution EPR spectrum of [Tp*MoO(S_2PEPP)] (red) and spectral simulation (blue). The isotropic EPR spectrum of [Tp*MoO(S_2PEPP)] indicates a small (~10%) Mo(V) impurity.

S3. Low temperature frozen glass EPR spectrum of [Tp*MoO(S_2PEPP)] (red) and spectral simulation (blue).

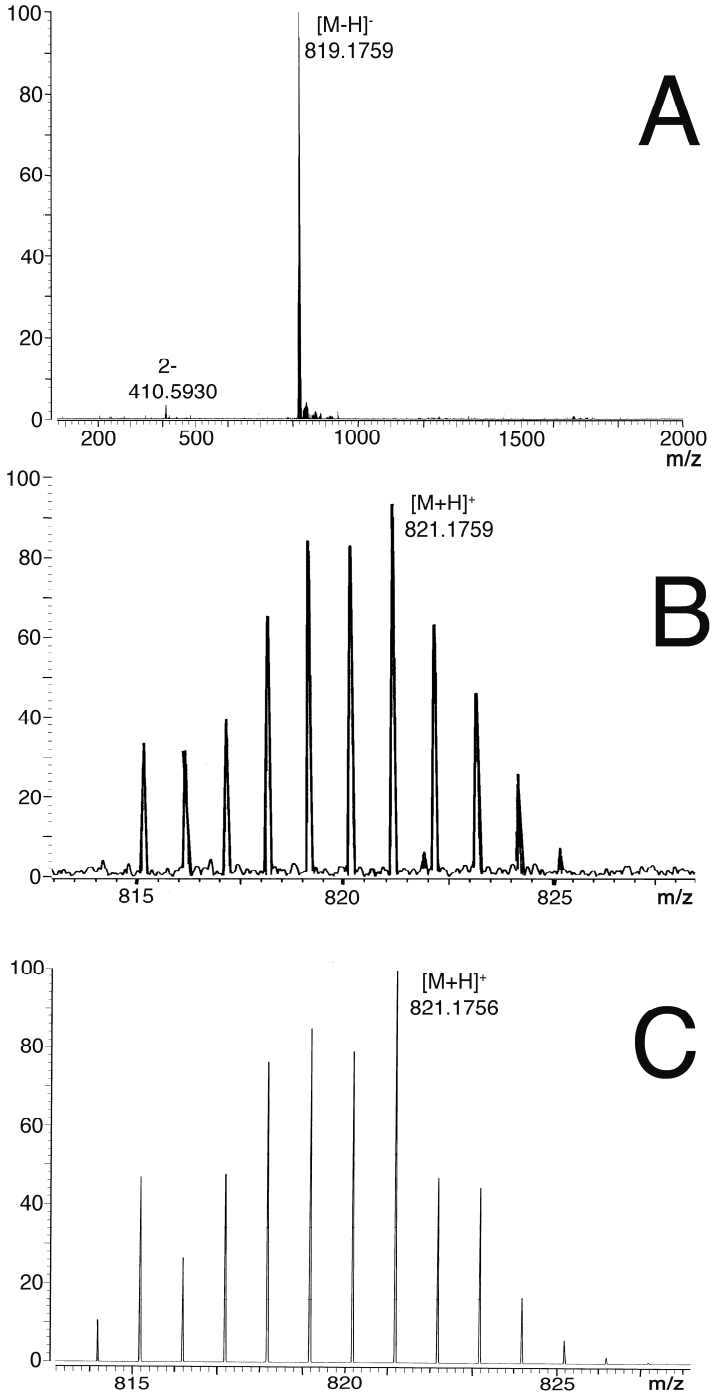
A
[M-H]-
819.1759
2-
410.5930
100
80
60
40
20
0
200
500
1000
1500
2000
m/z
B
[M+H]+
821.1759
815
820
825
C
[M+H]+
821.1756

S1

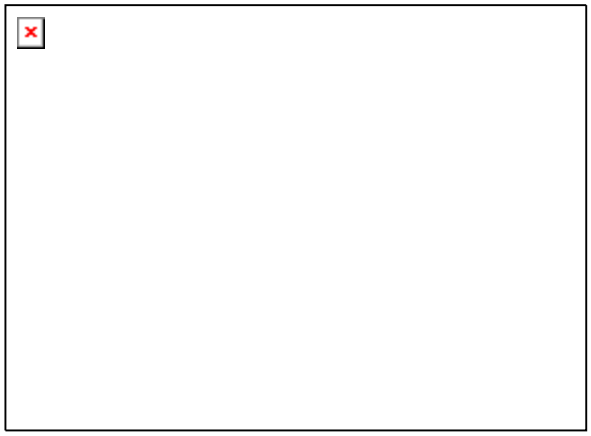

S2

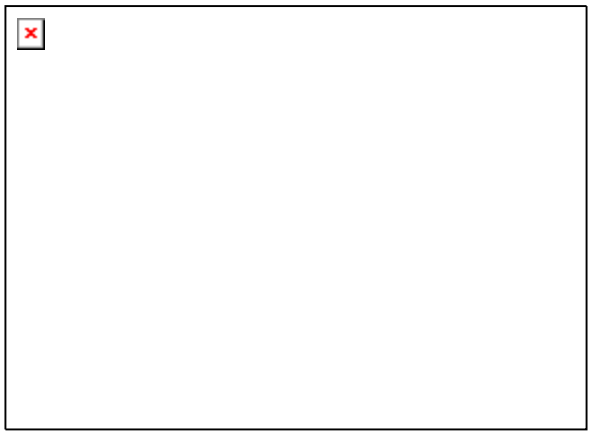

S3